NASA Tech Briefs

COMPLETE

National Aeronautics and Space Administration

99-05

May 1999

INTRODUCTION

Tech Briefs are short announcements of innovations originating from research and development activities of the National Aeronautics and Space Administration. They emphasize information considered likely to be transferable across industrial, regional, or disciplinary lines and are issued to encourage commercial application.

Availability of NASA Tech Briefs and TSPs

Requests for individual Tech Briefs or for Technical Support Packages (TSPs) announced herein should be addressed to

National Technology Transfer Center
Telephone No. **(800) 678-6882** or via World Wide Web at **www2.nttc.edu/leads/**

Please reference the control numbers appearing at the end of each Tech Brief. Information on NASA's Commercial Technology Team, its documents, and services is also available at the same facility or on the World Wide Web at **www.nctn.hq.nasa.gov**.

Commercial Technology Offices and Patent Counsels are located at NASA field centers to provide technology-transfer access to industrial users. Inquiries can be made by contacting NASA field centers and program offices listed below.

NASA Field Centers and Program Offices

Ames Research Center
Carolina Blake
(650) 604-0893 or
cblake@mail.arc.nasa.gov

Dryden Flight Research Center
Lee Duke
(805) 258-3802 or
lee.duke@dfrc.nasa.gov

Goddard Space Flight Center
George Alcorn
(301) 286-5810 or
galcorn@gsfc.nasa.gov

Jet Propulsion Laboratory
Merle McKenzie
(818) 354-2577 or
merle.mckenzie@ccmail.jpl.nasa.gov

Johnson Space Center
Hank Davis
(281) 483-0474 or
hdavis@gp101.jsc.nasa.gov

John F. Kennedy Space Center
Gale Allen
(407) 867-6626 or
galeallen-1@ksc.nasa.gov

Langley Research Center
Dr. Joseph S. Heyman
(804) 864-6006 or
j.s.heyman@larc.nasa.gov

Glenn Research Center
Larry Viterna
(216) 433-3484 or
ctt@lerc.nasa.gov

George C. Marshall Space Flight Center
Sally Little
(256) 544-4266 or
sally.little@msfc.nasa.gov

John C. Stennis Space Center
Kirk Sharp
(228) 688-1929 or
ksharp@ssc.nasa.gov

NASA Program Offices
At NASA Headquarters there are seven major program offices that develop and oversee technology projects of potential interest to industry:

Carl Ray
Small Business Innovation Research Program (SBIR) & Small Business Technology Transfer Program (STTR)
(202) 358-4652 or
cray@mail.hq.nasa.gov

Dr. Robert Norwood
Office of Aeronautics and Space Transportation Technology (Code R)
(202) 358-2320 or
rnorwood@mail.hq.nasa.gov

John Mulcahy
Office of Space Flight (Code MP)
(202) 358-1401 or
jmulcahy@mail.hq.nasa.gov

Gerald Johnson
Office of Aeronautics (Code R)
(202) 358-4711 or
g_johnson@aeromail.hq.nasa.gov

Bill Smith
Office of Space Science (Code S)
(202) 358-2473 or
wsmith@sm.ms.ossa.hq.nasa.gov

Roger Crouch
Office of Microgravity Science Applications (Code U)
(202) 358-0689 or
rcrouch@hq.nasa.gov

Granville Paules
Office of Mission to Planet Earth (Code Y)
(202) 358-0706 or
gpaules@mtpe.hq.nasa.gov

BLANK PAGE

NASA TechBriefs

May 1999
99-05

National Aeronautics and Space Administration

BLANK PAGE

Electronic Components and Circuits

Hardware, Techniques, and Processes

BLANK PAGE

6

Finite-Width Coplanar-Waveguide Patch Antenna

Developmental phased-array antennas would incorporate antenna elements like this one.

Lewis Research Center, Cleveland, Ohio

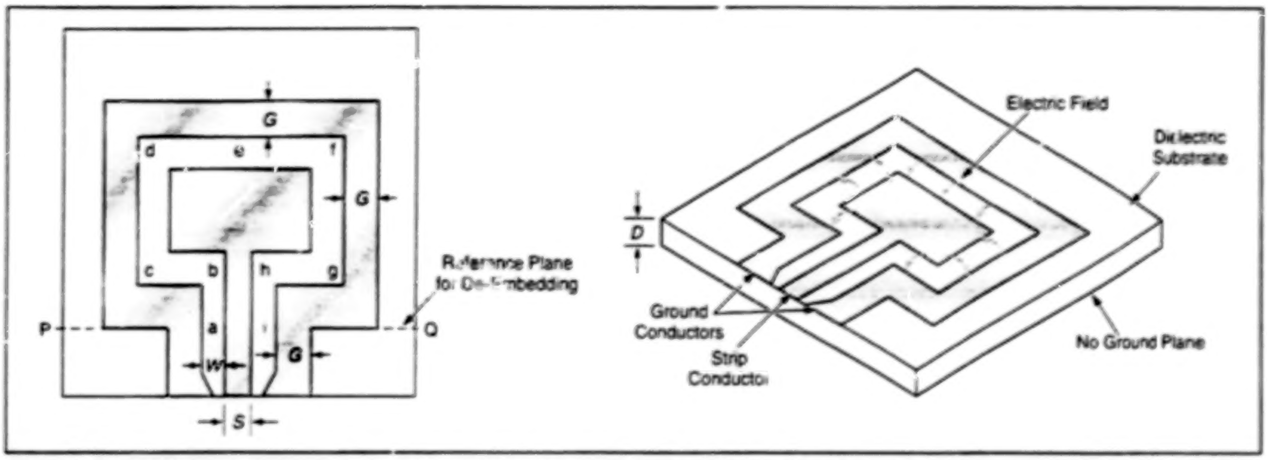

Figure 1. An **FCPW Patch Antenna** is derived by widening the middle strip conductor of a finite-width coplanar waveguide to form a rectangular patch.

The left part of Figure 1 illustrates an antenna derived by widening the middle strip conductor of a finite-width coplanar waveguide (FCPW) to form a rectangular patch. An FCPW offers all the advantages of a conventional coplanar waveguide, along with the additional advantage that its finite-width ground planes suppress the propagation of spurious substrate electromagnetic modes that would otherwise degrade the electrical performance of an array of patch antenna elements.

The lowest order of resonance of an FCPW patch antenna occurs at a frequency for which the guide wavelength, $\lambda_{g(slot)}$, equals the sum of mean lengths of slots from point a to point i. At resonance, the electric-field lines are oriented as shown by the curved arrows, and the antenna radiates with a polarization parallel to sides c–d and f–g.

An experimental FCPW antenna element like that of Figure 1 was fabricated by use of gold paste and screen printing on ceramic substrates. The substrate material had a relative permittivity of 5.9, making it possible to reduce patch dimensions significantly to make an array of such elements more compact. Dimensions included D = 0.01125 in. (0.286 mm), S = 0.012 in. (0.305 mm), W = 0.004 in. (0.102 mm), and G = 0.024 in. (0.700 mm). The input impedance of the antenna was measured by use of through-reflect-line on-wafer calibration standards, a pair of microwave probes, an automatic network analyzer, and de-embedding software from the National Institute of Standards and Technology; these measurements revealed that the antenna res-

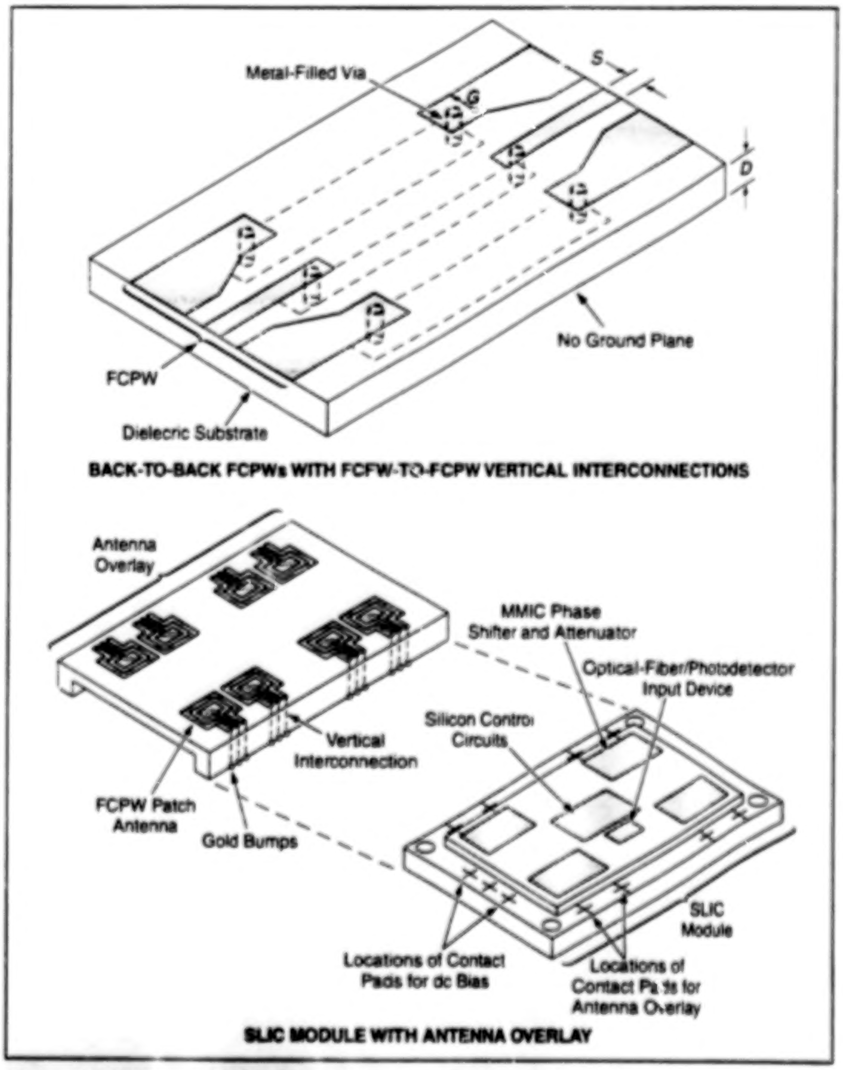

Figure 2. FCPWs and FCPW Patch Antennas are elements of developmental modules that will eventually be used to make compact phased-array antennas.

onated at frequency of 19.95 GHz with a de-embedded input impedance of 534 Ω at plane P–Q.

The upper part of Figure 2 illustrates two back-to-back FCPWs on the top side of a dielectric substrate, a connecting FCPW on the bottom side of the substrate, and FCPW-to-FCPW vertical interconnections (vias). An experimental unit having this configuration was made of substrate material and conductor strips with dimensions *D, S, W*, and *G* as described above, and with vias of ≈0.01 in. (≈0.25 mm) diameter.

The lower part of Figure 2 shows a system-level integrated circuit (SLIC) module that was undergoing development at the time of reporting the information for this article. The completed module would contain all the circuitry of an eight-element phased-array antenna. The module would contain four dual-channel monolithic microwave integrated circuits (MMICs) and supporting circuitry. Each of the dual channels would contain a three-bit phase shifter, an analog attenuator, and amplitude-calibration and -control elements. A photonic link would bring the radio-frequency signals and digital control signals into the module. Another photonic link would return information on the status of the module to an external controller.

This work was done by Richard Q. Lee and Kurt A. Shalkauser of **Lewis Research Center**; *Jonathan Owens, James Demarco, Joan Leon, and Dana Sturzebecher of PSD, Army Research Laboratory, AMSRL-PS-E; and Rainee N. Simons of NYMA, Inc. Further information is contained in a TSP [see page 1].*

Inquiries concerning rights for the commercial use of this invention should be addressed to NASA Lewis Research Center, Commercial Technology Office, Attn: Tech Brief Patent Status, Mail Stop 7–3, 21000 Brookpark Road, Cleveland, Ohio 44135. Refer to LEW-16666.

Resonant Microstrip Patch Antenna as Ice-Thickness Gauge

Conformally mounted sensors would measure prelaunch ice buildup on space-shuttle external tanks.

Lyndon B. Johnson Space Center, Houston, Texas

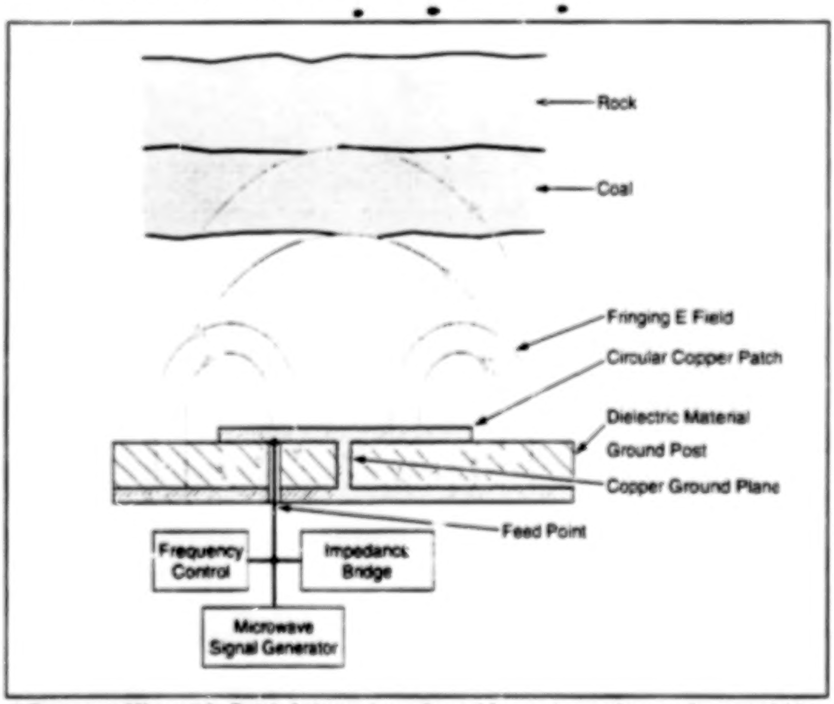

A Resonant Microstrip Patch Antenna is configured for use in sensing nearby material layers. The electric-field lines depicted here approximate those of the transverse magnetic 1,1 (TM11) mode.

Researchers at Johnson Space Center (JSC) recently demonstrated that the resonant microstrip patch antenna (RMPA), which has been proven in commercial applications, can be applied with equal success to measuring prelaunch ice buildup on the insulated low-temperature external tanks of the space shuttle orbiter. To do this, they explored the following questions: Why is prelaunch ice buildup on the shuttle external tanks measured, how is the ice measured now, how does the RMPA sensor work, and will the performance of this sensor satisfy the Space Shuttle Program launch-commit criteria.

Accurately measuring prelaunch ice buildup on the orbiter external tanks is a programmatic concern. After the tanks are filled, launch countdown continues unless the "acreage ice" builds to more than 1/16 in. (1.6 mm), at which point the applicable launch-commit criterion requires that the launch be delayed. The delay is necessary because, during initial ascent through the atmosphere, an ice layer thicker than 1/16 in. (1.6 mm) could become fragmented, causing damage to orbiter heat-shield tiles and windows. Therefore, the ability to measure the thickness of ice is vital to vehicle performance and safety. At present, ice measurements are performed on the launch pad, by teams of technicians who manually scratch away the ice layer to determine its thickness. However, the large size of external tanks limits accessibility and the number of measurements that can be taken in this way. A sensor that could automatically perform these measurements would increase accessibility and reduce risk.

JSC researchers needed a sensor that could be applied to the Shuttle's external tanks; the RMPA sensor and associated microprocessor-controlled electronic circuitry satisfied their need. But there was a drawback: Inasmuch as active circuits are essential parts of an RMPA sensor, operation of the circuits could, potentially, cause localized heating that could cause inaccurate measurements. Therefore, a multiple-element RMPA that could be integrated into the tank insulation was designed.

An RMPA sensor is driven by a microprocessor-controlled microwave signal generator. It is characterized by, among other things, an electric field (E field) distributed throughout a dielectric material between a circular copper patch and an underlying copper back plane (ground plane) through the dielectric material. The RMPA sensor can be modeled as a high-Q cavity (where "Q" denotes the resonance quality factor) that capitalizes on its

resonant sensitivity; this means that it offers a distinct advantage over a nonresonant electromagnetic (EM)-wave sensor.

The high-Q cavity is bounded by the circular copper patch and the ground plane. The E field within the cavity is both excited and sensed by use of a probe perpendicular to the ground plane at the feed point. An example of the E field within the cavity and the associated fringing E fields is illustrated in the figure. The magnetic (H) field, which is not shown in the figure, is orthogonal to the E field. The magnetic field in the vicinity of the edge of the circular patch is associated with currents that flow along the patch and ground-plane surfaces, and can be regarded as a diffuse magnetic boundary of the resonant cavity. The fringing E and H fields play an important role in the operation of the RMPA because they constitute the means for coupling between the internal cavity fields and the external fields.

The high-Q RMPA transmits primary electromagnetic fields and senses reflected and scattered electromagnetic fields through alteration of its resonant condition. The RMPA emits a continuous-wave signal that is partly reflected and partly transmitted at interfaces between layers of materials in and near the antenna, including layers of nearby materials (e.g., coal, rock, and/or ice) that one seeks to characterize.

The return signal, which is coupled through the fringing fields, alters the E field at the feed point. The microprocessor-controlled electronic circuitry of the RMPA changes the signal frequency until the measured impedance or admittance is real. The resonant resistance or conductance measured at the feed point can change by a significant amount when the layers of materials change.

The RMPA sensor has been proven useful in several commercial applications, for example, to measure the thickness of ice on a roadway, to measure the thickness of uncut coal in a mine, and as an ore-pass monitor. It should be possible to put the RMPA to good use in measuring ice buildup on the orbiter low-temperature external tanks. The replacement of measurements by technicians with measurements by RMPA sensors would make it possible to measure ice buildup on a greater portion of the tank surface in a timely manner; this would enable launch personnel to satisfy the applicable launch-commit criterion and to reduce the potential danger to the shuttle and its crew.

This work was done by Larry G. Stolarczyk of Raton Technology Research, Inc., for **Johnson Space Center**. *Further information is contained in a TSP [see page 1].*

In accordance with Public Law 96-517, the contractor has elected to retain title to this invention. Inquiries concerning rights for its commercial use should be addressed to

Larry Stolarczyk
Raton Technology Research
848 Clayton Highway
Raton, NM 87740

Refer to MSC-22766, volume and number of this NASA Tech Briefs issue, and the page number.

$LaNi_{5-x}M_x$ Alloys for Ni/Metal Hydride Electrochemical Cells

A systematic approach to extension of cycle lives has emerged from recent studies.

NASA's Jet Propulsion Laboratory, Pasadena, California

Studies of physical and chemical effects in the hydride-forming electrodes of rechargeable nickel/metal hydride electrochemical cells have yielded results that now guide efforts to formulate improved electrode alloys to extend the cycle lives of the cells. These efforts involve finding appropriate ternary solutes and amounts of those solutes to alloy with the original hydride-forming binary alloy $LaNi_5$ to form alloys of general composition $LaNi_{5-x}M_x$. Here, M denotes any suitable element or alloy that forms a strong bond with lanthanum, as explained below.

Findings consistent with this approach were reported in two previous articles in *NASA Tech Briefs*: "$LaNi_{5-x}Sn_x$ Electrodes for Ni/MH Electrochemical Cells" (NPO-19805) Vol. 22, No. 8 (August 1998), page 60 and "$LaNi_{5-x}Ge_x$ Electrodes for Ni/MH Electrochemical Cells" (NPO-19962), Vol. 22, No. 8 (August 1998), page 61. At the time of reporting the information for those articles, there was no explanation of the basic physical and chemical mechanisms for the degradation of cycle lives of $LaNi_5$ electrodes and for the improvements afforded by partial substitution of Sn or Ge for Ni. The basic mechanisms are still not well understood, but the following understanding has emerged from the research performed thus far:

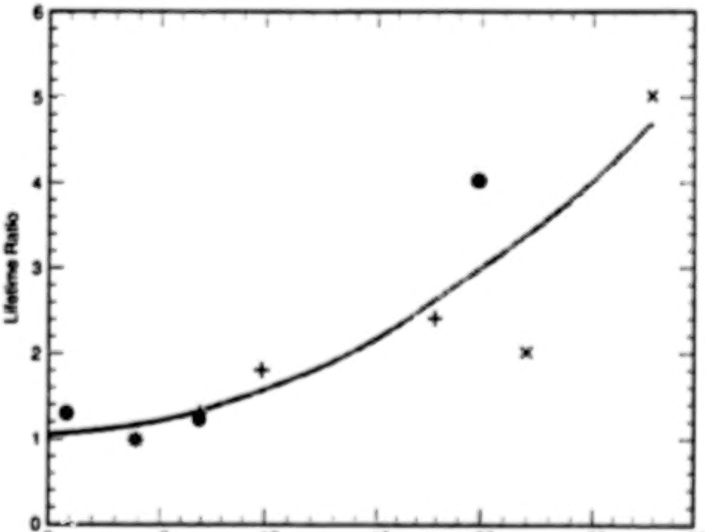

Cyclic Lifetimes of electrodes made of $LaNi_{5-x}M_x$ are related to heats of formation of M with La. The lifetime ratio for a given M is defined as (the number of charge-discharge cycles to half of initial charge capacity for an electrode made of $LaNi_{5-x}M_x$) ÷ (the corresponding number of cycles an electrode made of $LaNi_5$).

Hydrides of $LaNi_5$ are thermodynamically unstable against disproportionation reactions in which they decompose into Ni plus LaH_2 or $La(OH)_3$. In addition, upon

absorption of hydrogen, $LaNi_5$ can expand by as much as 24 volume percent; the combination of large expansion during absorption and the corresponding large contraction during subsequent desorption of hydrogen induces structural defects and reductions in particle sizes, with a consequent increase in the diffusion of metal atoms in the $LaNi_5$ crystalline lattice. This increase in diffusion increases the La content at the surface, where the La is readily oxidized to form a thick hydroxide layer in one of the disproportionation reactions. The present approach involving formulation of $LaNi_{5-x}M_x$ is based on suppressing diffusion of La and thereby preventing disproportionation of $LaNi_5$.

More specifically, the approach is to seek compositions and crystalline structures to immobilize lanthanum atoms in the Haucke-phase metal hydrides. The most promising ternary solutes for this purpose should be elements that form the strongest chemical bonds with lanthanum— stronger than the bonds between nickel and lanthanum. The solute atoms would be positioned on the nickel planes of the Haucke phase, so that they would be close to lanthanum neighbors. Strong bonds to neighboring atoms would suppress the formation of crystalline-lattice defects as well as movements of lanthanum atoms.

Preliminary support for this approach has been found through an analysis of cyclic lifetimes for various solutes as reported in the literature; the analysis reveals a close relationship between cyclic lifetime and the heat of formation of the solute with lanthanum (see figure). The finding of this relationship motivated the hypothesis that the rates disproportionation and/or degradation could be reduced by adding solutes that bond strongly with lanthanum. Among the solutes that exhibit high heats of formation with lanthanum are germanium and tin (mentioned in the cited prior articles), plus indium.

This work was done by Ratnakumar Bugga, Robert Bowman, Adrian Hightower, Charles Witham, and Brent Fultz of Caltech for **NASA's Jet Propulsion Laboratory**. *Further information is contained in a TSP (see page 1).*

In accordance with Public Law 96-517, the contractor has elected to retain title to this invention. Inquiries concerning rights for its commercial use should be addressed to

Technology Reporting Office
JPL
Mail Stop 122-116
4800 Oak Grove Drive
Pasadena, CA 91109
(818) 354-2240

Refer to NPO-20107, volume and number of this NASA Tech Briefs *issue, and the page number.*

Electronic Systems

Hardware, Techniques, and Processes

BLANK PAGE

12

Biotelemetry Using Implanted Unit To Monitor Preterm Labor

Pressure changes are telemetered to the outside and analyzed to detect intrauterine contractions.

Ames Research Center, Moffett Field, California

A biotelemetric system for monitoring key physiological parameters of a fetus and its uterine environment is undergoing development. The main purpose of the monitoring is to detect preterm labor in order to enable timely treatment. At the present stage of development, the system monitors pressure changes and temperature. The pressure changes serve as direct indications of intrauterine contractions that could be associated with the onset of preterm labor. Future versions of the system are expected to monitor additional parameters, including pH and the heart rate of the fetus.

The system (see Figure 1) includes a transmitting unit that contains a thermistor (the temperature sensor) and a piezoresistive transducer (the pressure sensor), a receiver, data-acquisition subsystem, and a digital signal-processing subsystem. The fully developed transmitting unit is projected to be small enough that it could be introduced into the uterine cavity through a 10-mm trocar during endoscopic fetal surgery; the surgical procedure for implanting this transmitter would be less invasive than are the hysterotomies performed to implant the transmitting units of telemetric systems developed previously for the same purpose.

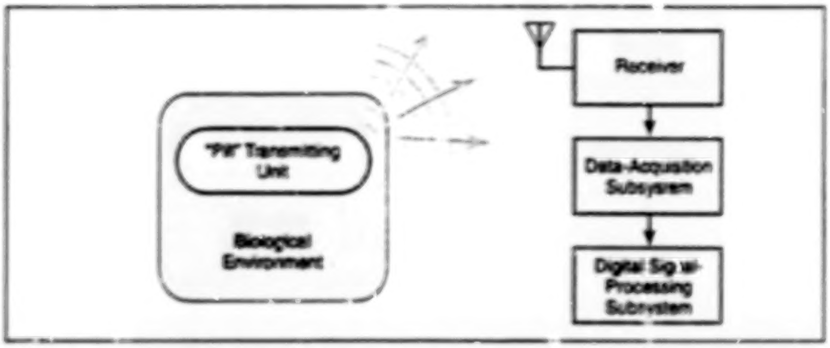

Figure 1. A **Transmitting Unit in a Uterus** monitors physiological parameters and transmits its readings to external equipment. The fully developed transmitting unit, resembling a large pill, would be small enough to be implantable by minimally invasive surgery.

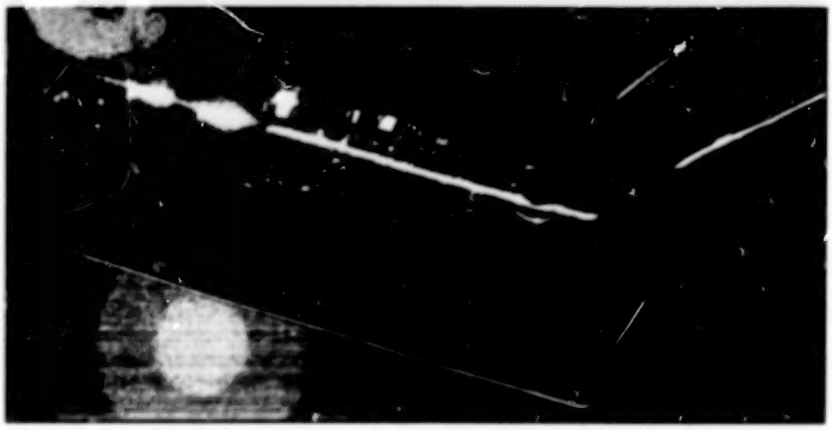

Figure 2. A **Prototype Transmitting Unit** would be miniaturized and encapsulated in biocompatible silicone rubber.

The transmitter generates a pulsed signal at a carrier frequency between 174 and 214 MHz. The temperature and pressure information are conveyed by pulse-interval modulation (PIM): Pulses are transmitted in pairs at a pulse-pair-repetition frequency of about 1 to 2 Hz. The interval between the two pulses in each pair is proportional to the sensed pressure, while the interval between pairs is proportional to the departure of the sensed temperature from a predetermined nominal value. The low data rate is sufficient for monitoring intrauterine contractions, which typically occur over several minutes. The transmission range is 3 to 10 ft (1 to 3 m), depending on the position of the transmitter in the body.

Transmitter power is supplied by two silver oxide batteries; at an average power consumption <40 μW, the operational lifetime ranges from 4 to 6 months. The fully developed transmitting unit would be electronically identical to a larger prototype that has already been constructed (see Figure 2), but would be miniaturized by following the chip-on-board approach, in which unpackaged integrated-circuit chips are flip-chip bonded directly onto a printed-circuit board along with other components. The transmitter is encapsulated in biocompatible silicone rubber.

The receiver converts the PIM radio-frequency signal into a digital pulse stream, which is then decoded to obtain voltages proportional to the temperature and pressure readings. These voltages are digitized in the data-acquisition subsystem, which is a Personal Computer Memory Card Association (PCMIA) circuit card in a laptop computer. The digital data are then processed in the digital signal-processing system, which is the remainder of the laptop computer.

The processing is done by a LabVIEW® program that displays and stores the pressure and temperature data as functions of time, performs peak detection, and determines the frequency of contractions. The program integrates the pressure over time to obtain an index of the amount of preterm labor. A unique feature of the program is the application of statistical and frequency-analysis functions to the pressure data to help a pediatric surgeon detect preterm labor. Among other things, the program displays the frequency spectrum of intrauterine contractions. Another unique feature is a contraction-detecting algorithm.

This work was done by John W. Hines of **Ames Research Center** *and Christopher J. Somps, Robert D. Ricks, and Carsten W. Mundt of Sverdrup Technology, Inc. Further information is contained in a TSP [see page 1].*

Inquiries concerning rights for the commercial use of this invention should be addressed to the Patent Counsel, Ames Research Center [see page 1]. Refer to ARC-14280.

Compact Magnetic-Sensor Units for Detecting Mines

Inexpensive, mass-produced units would be deployed in large numbers.

NASA's Jet Propulsion Laboratory, Pasadena, California

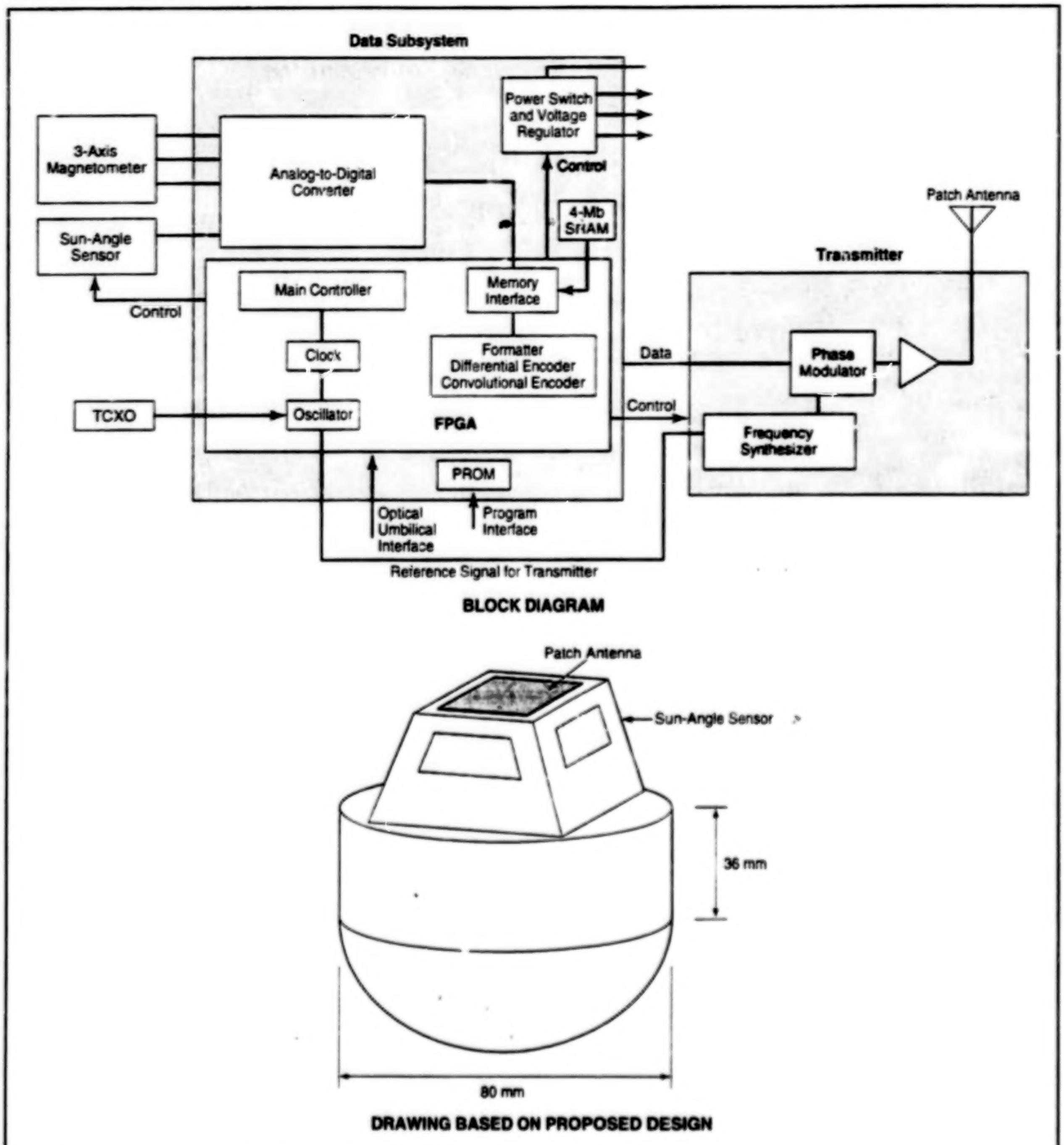

This **ISS Unit** is one of many that would be dispersed over the ground to detect magnetic-field anomalies caused by mines.

Compact, low-power-consumption magnetic-sensor units called "integrated sensor system" (ISS) units are being developed for detecting buried mines and arsenals without exposing human searchers to unnecessary danger. The fully developed ISS units would be mass produced at relatively low cost, so that they could be deployed in large numbers and regarded as disposable. Many ISS units would be dispersed onto a mine field from a low-flying aircraft. After a specified time, the ISS units would transmit magnetic-field- and attitude-measurement data to the same or different aircraft for processing. Analysis of the data would reveal local deformations of the Earth's magnetic field, indicative of the magnetic dipole moments of mines and other objects.

Each ISS unit (see figure) would contain a miniature three-axis flux-gate magnetometer, a Sun-angle sensor, a data subsystem, a battery power subsystem, a transmitter, and a patch antenna. The

ISS unit would be packaged with non-magnetic components. The entire unit would be designed with great care to ensure that the magnetometer readings would not be corrupted despite the proximity of the magnetometer to the electronic circuitry and packaging.

The three-axis magnetometer chosen for the ISS is one that was recently developed for use in an airborne unit. It includes low-noise ferromagnetic cores with windings for the three axes, plus drive and read-out circuits made of commercially available components.

The Sun single sensor, designed previously for use on small satellites, is a wide-angle optoelectronic sensor module in a pyramidal housing. The angle of the Sun, relative to the unit, is deduced from differences among the currents generated by four solar photovoltaic cells.

The data subsystem would include a 22-bit analog-to-digital (A/D) converter. The flow of data and the general operation of the rest of the ISS unit would be controlled by a field-programmable gate array (FPGA). A 4-Mb static random-access memory (SRAM) would store data (typically about 7 minutes' worth) until transmission. Data would not be acquired during transmission because operation of the transmitter could corrupt the magnetometer readings.

The battery power subsystem would include six high-capacity $Li/SOCl_2$ cells, plus power-regulation circuitry that is part of the data subsystem. Once activated, the ISS unit would continue to operate until the battery runs down (nearly two hours).

The transmitter would operate at a center frequency of 2,250 MHz. It would contain a frequency synthesizer in the form of a voltage-controlled oscillator locked in phase with a temperature-controlled crystal oscillator (TCXO). The output of the frequency synthesizer would be phase-modulated with the data signal, then amplified, then fed to the patch antenna.

Future refinements of the ISS design would effect increases in magnetic sensitivity, making it possible to detect mines with smaller magnetic moments. Of course, the magnetic-field-based ISS units would not be capable of detecting mines constructed entirely of nonferrous materials. On the other hand, they can be expected to detect a variety of mines of a low-technology type that are built at clandestine factories and have large magnetic moments. As newer mines are made with ever weaker magnetic moments, the basic ISS design could be modified to incorporate electronic chemical sensors to detect explosive vapors.

This work was done by Hamid Javadi of Caltech for **NASA's Jet Propulsion Laboratory**. *Further information is contained in a TSP* *[see page 1].*
NPO-20471

GPS "Compound Eye" Attitude Sensor

Attitude within several degrees would be determined relatively easily.

Goddard Space Flight Center, Greenbelt, Maryland

A proposed Global Positioning System (GPS) sensor would give information on approximate attitude as well as on position. Unlike other GPS-based attitude sensors, this attitude sensor would not depend on carrier-phase measurements and thus would not be subject to the difficulties and limitations involved in determining attitude from such measurements. Instead, this attitude sensor would be based on a concept that is related to that of an insect's compound eye and that has been implemented in optical attitude sensors of the star-tracker type.

The sensor would be equipped with multiple directional antennas mounted on a convex hemispherical surface. The number of antennas and their locations on the surface would be chosen to obtain a regular or slightly irregular polyhedral (e.g., half-dodecahedral or half-icosahedral) arrangement. Each antenna would thus be aimed to receive GPS signals from a field of view, called a "visualization cone," approximately coincident with the solid angle intercepted by the corresponding face of the polyhedron from the center of the hemisphere (see figure).

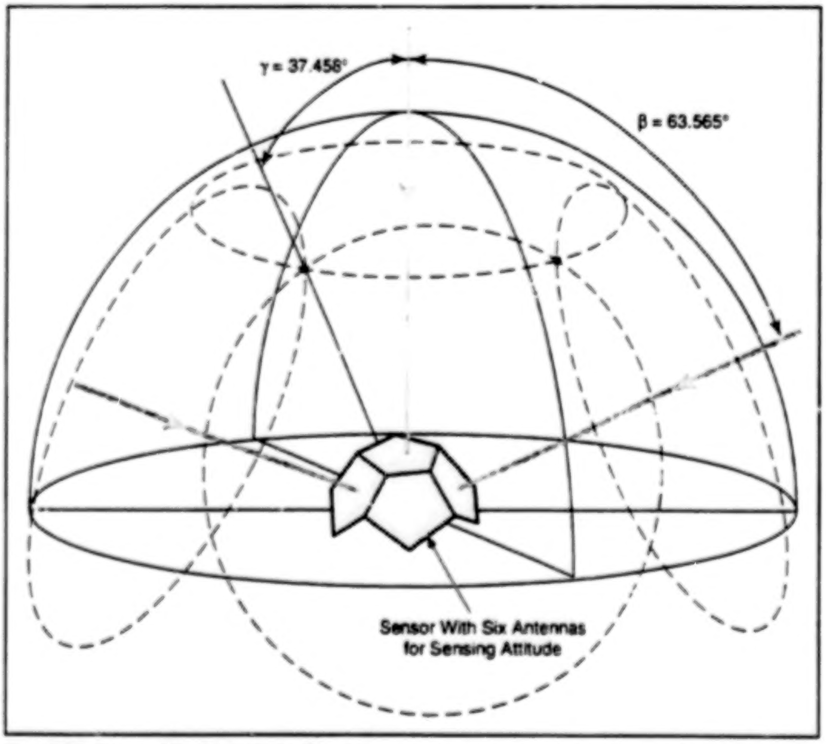

This GPS Sensor Would Include Six Antennas aimed outward from faces of a half regular dodecahedron. Their fields of view would be partially overlapping "visualization cones." The purpose of this arrangement is to deduce the orientation of the sensor from the known location of each GPS satellite "visible" to each antenna.

By virtue of the conventional GPS function, the positions of the GPS satellites and of the sensor would be known accurately and thus the direction from the sensor to each GPS satellite would be known accurately. Therefore, the reception of a signal from a given GPS satellite or satellites through a given antenna would provide partial attitude information: it would signify that the sensor is oriented so that the visualization cone of the given antenna contains the known direction(s) to the

satellite(s). In a similar manner, the simultaneous reception of GPS signals through the other antennas would make it possible to draw additional conclusions as to how the sensor must be oriented in order to make possible the observed combination of antennas and signals.

The precision of the attitude estimate obtained in this way depends on a number of factors, including notably the number of antennas and the way in which the signal-reception data are processed. Simplistic processing of raw data yields attitude estimates with errors of the order of visualization-cone angles (tens of degrees in the case of a half-dodecahedron). Errors can be reduced by use of optimization techniques in which, for example, greater weights are assigned to signals from directions that lie in overlaps between cones. Errors could be reduced further by increasing the number of antennas to obtain smaller cone angles and overlaps; for example, a first-order calculation has shown that with 16 antennas distributed over the hemispherical surface (on a "buckeyball"), errors would be reduced to <3°. Refinements in processing should make it possible to reduce the errors to the subdegree range.

This work was done by David A. Quinn of **Goddard Space Flight Center** *and John C. Crassidis of Texas A & M University. Further information is contained in a TSP [see page 1].*

This invention is owned by NASA, and a patent application has been filed. Inquiries concerning nonexclusive or exclusive license for its commercial development should be addressed to the Patent Counsel, Goddard Space Flight Center [see page 1]. Refer to GSC-13966.

Physical Sciences

Hardware, Techniques, and Processes

BLANK PAGE

18

Single-Crystal YAG Reinforcement Preforms for Refractory Composites

Preforms can be made in net size and shape, with tailored orientation of fibers.

Lewis Research Center, Cleveland, Ohio

Preforms (essentially, shaped mats) of single-crystal yttrium aluminum garnet (YAG) fibers can now be readily fabricated in net size and shape, with tailored orientation of the fibers. These preforms can be used as fiber reinforcements in ceramic- and metal-matrix composite materials that withstand temperatures as high as 1,700 °C. The development of these preforms and composites is a continuing effort in conjunction with other efforts to develop lightweight components for aircraft turbine engines.

The single-crystal form of YAG is needed for creep resistance; the polycrystalline forms of YAG and other oxide fiber materials do not resist creep adequately at the contemplated high operating temperatures. It would be expensive and impractical to construct preforms by weaving, braiding, or laminating premanufactured single-crystal fibers, and handling of the fibers during such construction would weaken them.

A proprietary process is being developed to overcome the above-mentioned limitations. In this process, reinforcement preforms are formed to net-shape, eliminating the need for operations such as weaving and braiding of single filaments. The net-shape preforms can have random, oriented, or mixed reinforcement in selective areas. Reinforcement volume-fraction shape and orientation can be controlled. Thin complex parts such as airfoils can be fabricated. Single-crystal porous preforms with volume percent in the range of 30 to 54 percent and strut dimensions in the range of 10 to 125 micrometers have been produced.

Figure 1 shows a scanning electron micrograph of porous single-crystal YAG reinforcement. Figure 2 shows a Laue x-ray diffraction pattern from this porous YAG preform. The Laue x-ray pattern is characteristic of single-crystal YAG, thus proving its single-crystal nature. High magnification microscopy indicated the absence of grain boundaries and confirmed the single-crystal nature. Reinforcement preforms with random, unidirectional and [0/90] reinforcement have been fabricated so far. Sufficient permeability of the preforms was demonstrated by conducting infiltration of the preform by polymer and metal matrices by pressure infiltration. Work is underway to optimize the preform reinforcing efficiency and infiltration with ceramic and intermetallic matrices.

Porous single crystals made by this proprietary approach also have applications such as selective emitters, filters, and photonic band-gap materials due to their unique physical properties. Porous single crystals of sapphire, YAG, eutectic YAG, doped sapphire, ytterbia have been fabricated by this process and potential exists for fabricating porous single crystals of many other materials.

This work was done by Prashant G. Karandikar, Ronald Roy, and Uday Kashalikar of Foster-Miller, Inc., for **Lewis Research Center**.

Inquiries concerning rights for the commercial use of this invention should be addressed to NASA Lewis Research Center, Commercial Technology Office, Attn: Steve Fedor, Mail Stop 4-8, 21000 Brookpark Road, Cleveland, Ohio 44135. Refer to LEW-16665.

Figure 1. A **Scanning Electron Micrograph** shows a random porous single-crystal YAG.

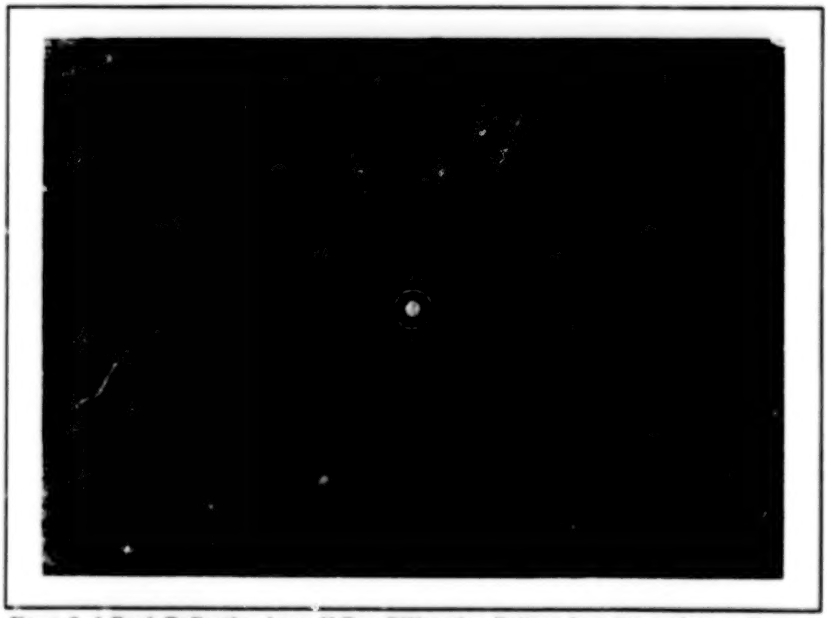

Figure 2. A **Back-Reflection Laue X-Ray Diffraction Pattern** from the preform in Figure 1 confirms its single-crystal nature.

Acoustical-Sensor Assemblies for Use in Flows

Screens and absorbers reduce spurious signals.

Ames Research Center, Moffett Field, California

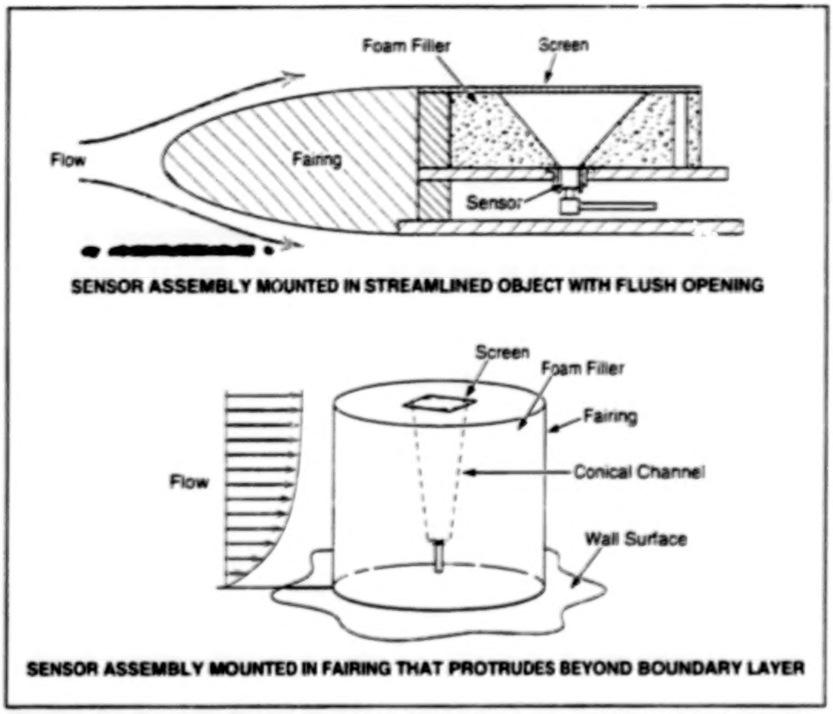

Sensors Are Mounted Behind Screens at the apices of conical holes in sound-absorbing foam fillers.

Improved sensor assemblies have been invented for measuring acoustic signals in gases or liquids flowing in or around any of a variety of moving or stationary objects. Examples of such objects include land vehicles, aircraft, submarines, structures exposed to winds or natural water streams, and industrial equipment containing or surrounded by process streams. In comparison with older acoustical-sensor assemblies designed for use in flows, these assemblies offer reduced response to noise generated by flows at and near sensor-assembly surfaces and increased protection for fragile acoustical transducers. These assemblies can be made to discriminate against sounds coming from outside preferred ranges of directions. They can also be mounted flush with surfaces of objects to minimize flow-induced noise and drag.

The figure illustrates two assemblies within the scope of the invention. In each case, the sensor is a microphone or other dynamic-pressure transducer. Each sensor is mounted in a cavity, wherein it is recessed from a streamlined surface. The cavity is lined with a sound-absorbing foam filler. A hole in the filler tapers conically from the sensor at its narrow end to an opening on the streamlined surface at its wide end. The cone angle is chosen, along with other design parameters, to obtain the desired directional response.

The opening on the streamlined surface is covered with a screen or porous sheet, which prevents or reduces the propagation of surface-flow disturbances (turbulence) into the cavity while allowing the acoustic waves of interest to propagate to the sensor. The placement of the sensor in the recess behind the screen thus reduces the intensity of flow-induced noise arriving at the sensor. Moreover, spurious acoustic disturbances arriving from immediately upstream or downstream of the opening can be rejected by reflection from the shear layer in the flow adjacent to the screen. Because the fluid in the cavity is still or nearly still, relative to the fluid outside the cavity, the sensor is protected against damage by the flow. The screen also protects the sensor against impacts of particles entrained in the flow.

The sensor assembly shown in the upper part of the figure is mounted inside a streamlined body with a rounded fairing on its upstream end, for measuring sounds arriving at the surface of the body. The sensor assembly shown in the lower part of the figure is mounted on the wall of an object; this sensor assembly includes its own fairing, which protrudes into the flow beyond the wall boundary layer or free shear layer, for measuring sounds free of interference from turbulence in this layer.

This work was done by Fredric Schmitz, Sandy Liu, Stephen Jaeger, and W. Clifton Horne of **Ames Research Center**. *Further information is contained in a TSP [see page 1].*

This invention has been patented by NASA (U.S. Patent No. 5,684,756). Inquiries concerning nonexclusive or exclusive license for its commercial development should be addressed to the Patent Counsel, Ames Research Center [see page 1]. Refer to ARC-12099.

Inflatable Membrane Reflectors for Multiple-Purpose Applications

Attention to details of design and modeling could result in fairly precise surfaces.

NASA's Jet Propulsion Laboratory, Pasadena, California

Experiments have demonstrated the feasibility of inflatable reflectors with very low system aerial densities of the order of 1 kg/m^2. Diverse applications include radio and optical communications, telescopes, and the concentration of sunlight for power generation. The same technology can be used for structural beams in single or multiple layers with excellent rigidity. Development work thus far has focused on potential uses in outer space, but inflatable rigidized structural elements are suitable for terrestrial applications where large lightweight surfaces and structures are needed.

The basic concept of an inflatable reflector is simple: stretch a membrane beyond its elastic limit by using a combination

mechanical tensioning and pressure. The shape the resulting surface takes is a good approximation to an ellipse with higher order correction terms. The shape can be modified by changing the boundary, the pressure, or the membrane material. A change in area of approximately 1 percent is required to plastically deform the membrane into the desired shape. After forming, the pressure is released with the resulting surface being a self-supporting membrane reflector. For imaging applications, the aberrations induced by the membrane reflector could be compensated for [illegible] design problem is to choose the membrane material and boundary conditions to obtain the desired reflector shape.

The figure shows an experimental apparatus on which a stainless steel membrane is stretched across a circular boundary and pressurized. The result is a smooth, rigid, self-supporting curved reflector surface of a quality suitable for use as a mirror in the far-infrared or submillimeter wavelengths (measured surface 8 micrometers root-mean square [RMS] over the central 40 cm of the membrane). The global surface figure can be adjusted by changing the pressure, the stretching forces, or the boundary over which the membrane is stretched.

A Stainless Steel Membrane is stretched across a circular boundary and pressurized to deform it into a curved mirror.

This work was done by Neville Marzwell of Caltech and Mark Dragovan of the Fermi Institute, University of Chicago, for **NASA's Jet Propulsion Laboratory.** *Further information is contained in a TSP [see page 1].*

NPO-20359

Quadrupole Mass Analyzer Based on Linear Ion Trap

Size, mass, and power consumption would be reduced, relative to traditional QMAs.

NASA's Jet Propulsion Laboratory, Pasadena, California

An improved quadrupole mass analyzer (QMA) has been proposed for use in determining the compositions of gas mixtures. The proposed QMA would incorporate two major innovations over traditional QMAs: (1) It would feature a simplified radio-frequency-excited quadrupole electrode structure that would be smaller, weigh less, and consume less power, relative to the quadrupole electrode structure of the corresponding traditional QMA; and (2) it would include dc end electrodes that would enable it to function as either a traditional transmission-mode mass spectrometer or an ion-trap mass spectrometer (ITMS).

The figure illustrates the proposed quadrupole electrode configuration and the corresponding traditional configuration, both designed for an inner radius r_0. In the traditional configuration, the outer cylindrical electrode is grounded, while a radio-frequency signal of amplitude V_0 is applied in opposite polarities to successive rod electrodes at 90° angular intervals. The radius of the quadrupole electrodes ($1.1468r_0$) and the radius of the outer shielding electrode ($3.54r_0$) are chosen to eliminate a sixth-order departure from the ideal quadrupolar electric potential and thereby obtain a close approximation to the ideal quadrupolar electric field.

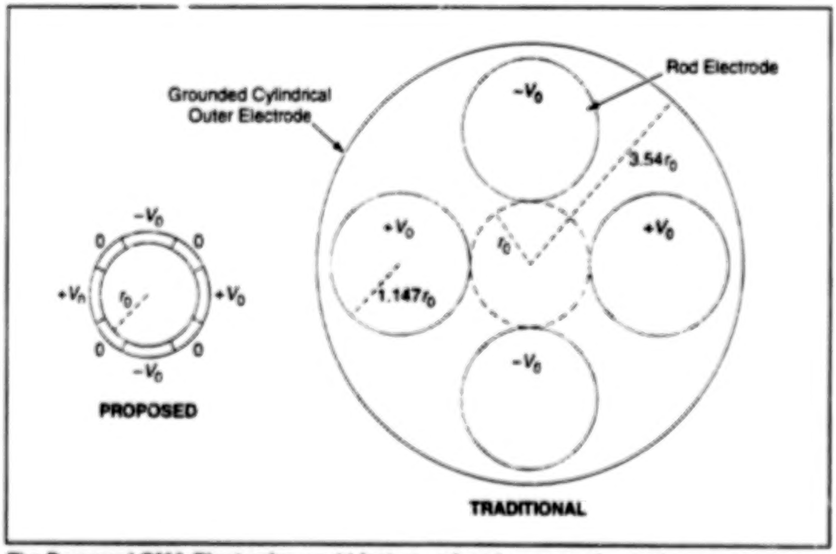

The Proposed QMA Electrodes would feature reduced cross section and power consumption, relative to the corresponding traditional QMA electrodes.

The proposed quadrupole electrodes would be made from a single, precisely machined hollow cylinder cut lengthwise into eight sectors with alternating angular widths of 30° and 60°. The 30° sectors

would be electrically grounded, while the radio-frequency signal of amplitude V_0 would be applied in opposite polarities to successive 60° sectors. This configuration would also eliminate the sixth-order departure from the ideal quadrupolar potential, yielding a similar close approximation to the ideal quadrupolar electric field. A simple comparison of overall radii shows that the cross-sectional area of the proposed QMA would be less than 1/10 that of the traditional QMA. If the proposed and traditional QMAs were of the same length, then the proposed QMA could be made to weigh about 1/10 as much.

Further analysis of the electric fields reveals that the proposed QMA could achieve the same stability parameters as does the traditional QMA at an excitation voltage about 10 percent smaller, and that the capacitance of the proposed QMA would be about 1/4 that of the traditional QMA. As a result, the energy stored in the electric field of the proposed QMA would be only about 1/5 that of the traditional QMA. As a further result, if the resonance quality factors of the excitation circuits were the same in both cases, the proposed QMA would consume only about 1/5 the power of the traditional QMA.

The ITMS version of the proposed QMA would be based on a linear ion trap, in which the trapping volume would be roughly a cylinder of length L and small characteristic radius R about the axis of symmetry. In contrast, a traditional ITMS is based on a point-node ion trap, in which the trapping volume is roughly a sphere of radius R. Thus, the trapping volume of the proposed ITMS version would be about $3L/4R$ times that of a traditional ITMS. One could choose the dimensions of the electrodes to obtain $L >> R$, such that the trapping volume of the proposed ITMS version would be 100 to 1,000 times the volume of the corresponding traditional ITMS; the number of ions generated and trapped would be increased accordingly.

This work was done by John D. Prestage of Caltech for **NASA's Jet Propulsion Laboratory**. *Further information is contained in a TSP [see page 1].*

In accordance with Public Law 96-517, the contractor has elected to retain title to this invention. Inquiries concerning rights for its commercial use should be addressed to

Technology Reporting Office
JPL
Mail Stop 122-116
4800 Oak Grove Drive
Pasadena, CA 91109
(818) 354-2240

Refer to NPO-20011, volume and number of this NASA Tech Briefs *issue, and the page number.*

Computing Chemical Kinetics With Low-Dimensional Manifolds

This method can be used to predict the concentration of NO_x in combustion exhaust.

Lewis Research Center, Cleveland, Ohio

Case Number	Predicted Concentration, Parts Per Million	Measured Concentration, Parts Per Million
1	20.5	21.6 to 26.5
2	6.9	10.6
3	4.9	12.0
4	13.9	3.1
5	28.5	35.1

Concentrations of NO_x as predicted by the present method approximated those measured in experiments in five test cases of combustion of hydrogen jets injected radially into a can downstream of an air inlet. The differences between predicted and experimental values for cases 2 through 5 should be analyzed with caution because the CFD computations for those cases were not carried out to full convergence.

A method of computing the concentrations of chemical species in chemically reacting flows includes, among other things, utilization of a prior chemical-kinetic method based on a concept of intrinsic low-dimensional manifolds (ILDM) in composition space. The present method is particularly suitable for predicting concentrations of nitrogen oxides (NO_x) generated in the combustion of hydrocarbon fuels in flows simulated by techniques of computational fluid dynamics (CFD).

The composition of a chemical system can be regarded as a point in composition space, which is a multidimensional space in which each dimension represents the concentration of one of the chemical species present. The chemical-kinetic rate equations of the system can be regarded as representing how the composition point moves in the space. In a typical case, the composition changes much more rapidly in some dimensions than in others, so that the composition point can be regarded as (1) first moving rapidly toward an attracting manifold of reduced dimensionality (for example, a surface in space of three or more dimensions), then (2) moving along the manifold toward an equilibrium point.

In the ILDM method, one identifies such a manifold, assumes that the composition always lies on the manifold, and uses the reduced dimensionality of the manifold to reduce the amount of computation needed to solve the corresponding equations of chemical kinetics. One still accounts for all of the chemical species of a complex system, but takes advantage of the simplification to parameterize the system by use of relatively few variables. In principle, the manifold can be identified once the number of its dimensions is known or assumed.

In the present method, the ILDM method is implemented by a computer code that automatically identifies a manifold on which a simplified mathematical model of a chemical system is parameterized by two variables: (1) a mixture fraction that is a function of mass fractions of species present in the system and (2) a progress variable, which can be either another function of species mass fractions, a temperature, or a Gibbs function. The only restriction on the choice of the progress variable is that this variable must be a single-valued function in the given system. The resulting species concentrations, rates, and properties are stored in look-up tables. These tables can then be used as the chemistry model in CFD calculations. By using look-up tables, the calculation of properties and reaction rates is replaced by interpolation, resulting in significant savings in central processing unit (CPU) time.

The method can also be used to post-process results of CFD simulations of reacting flows and, in particular, of flows in combustors burning hydrocarbon fuels in air. Typically, a CFD code yields the flow

velocities, temperatures, and concentrations of the major chemical species (fuel, O_2, N_2, H_2O, CO, and CO_2). For each node on a computational grid, the mixture fraction and progress variable can be calculated from the CFD output data. Then with the help of interpolation routines that can be called from the CFD code, the mixture fraction and progress variable can be used to obtain concentrations of such minor species as NO_x (see table). This computation amounts to a mapping procedure that can be accomplished rapidly; computations for a million nodes take only a few minutes.

This work was done by A. T. Norris of the Institute for Computational Mechanics in Propulsion for **Lewis Research Center**. *Further information is contained in a TSP [see page 1].*

Inquiries concerning rights for the commercial use of this invention should be addressed to NASA Lewis Research Center, Commercial Technology Office, Attn: Tech Brief Patent Status, Mail Stop 7-3, 21000 Brookpark Road, Cleveland, Ohio 44135. Refer to LEW-16659.

BLANK PAGE

24

Materials

Hardware, Techniques, and Processes

Books and Reports

BLANK PAGE

Ceramic Composites of ZrB_2, HfB_2, ZrC, HfC, and SiC

These ceramics offer superior resistance to ablation at high temperature.

Ames Research Center, Moffett Field, California

Improved zirconium- and hafnium-based ceramic composites have been invented in an effort to obtain better resistance to ablation at high temperature. These ceramics are suitable for use as thermal-protection materials on the exterior surfaces of spacecraft reentering the terrestrial atmosphere, and in laboratory and industrial environments that include flows of hot oxidizing gases.

The predecessors of these ceramic composites are ZrB_2/SiC and HfB_2/SiC composites, which exhibit high resistance to oxidation and thermal shock, high configurational stability, and high resistance to ablation. The ablation resistance of ZrB_2/SiC and HfB_2/SiC composites is believed to arise from the formation of coherent passivating oxide scales on their surfaces. However, each such composite exhibits a transition point within its operational envelope of mach number vs. stagnation heat flux; beyond this point, the cohesiveness of the oxide scale decreases in such a way that microspallation of the oxide scale and concomitant accelerated conversion occur. Thus, resistance to ablation decreases beyond the transition point. The present innovative ceramic composites offer superior resistance to ablation.

A ceramic of the present type is a multiphase composite of (1) zirconium diboride and zirconium carbide with silicon carbide, (2) hafnium diboride and hafnium carbide with silicon carbide, or (3) mixed diborides and/or carbides of zirconium and hafnium with silicon carbide. The composite material is made by sintering a mixture of the metal diboride, metal carbide, and silicon carbide powders at a temperature of about 1,900 °C or greater. Typical composition ranges in volume percentages of the starting ceramic powders are the following:

Constituent	Proportion, Volume Percent
ZrB_2 and/or HfB_2	20 to 64
ZrC and/or HfC	20 to 64
SiC	≤20 (Preferably 10 to 16)

A given composition is said to be diboride- or carbide-rich, depending on the ratio between the metal diboride and metal carbide contents.

Figure 1 is a pseudo-ternary phase diagram for the special case of composites made from either (1) ZrB_2, ZrC, and SiC or (2) HfB_2, HfC, and SiC but not (3) mixtures of the diborides and/or carbides of both Zr and Hf. "Pseudo-ternary phase diagram" as used here signifies that the three points of the triangle represent the starting ZrB_2 or HfB_2, ZrC or HfC, and SiC components, as distinguished from a true ternary diagram in which the individual elements Zr or Hf, Si, and C are represented. The composition ranges stated above are represented by the shaded trapezoidal area.

The table in Figure 2 presents some results of a test in which two composites of the present type and two of the previous type were exposed to an arc jet at a heat flux of 400 W/cm². The results show that with respect to conversion rates, the present ceramic composites resist ablation or conversion better than do the corresponding predecessor ZrB_2/SiC and HfB_2/SiC composites. The results are even more impressive when densities and surface temperatures are taken into account: About 50 seconds into the test, the ZrB_2/SiC ceramic underwent a transition in which the surface temperature rapidly climbed to a maximum of 2,200 °C, with resultant micro and macro spallation, and stability was not reestablished.

This work was done by Jeffrey Bull of

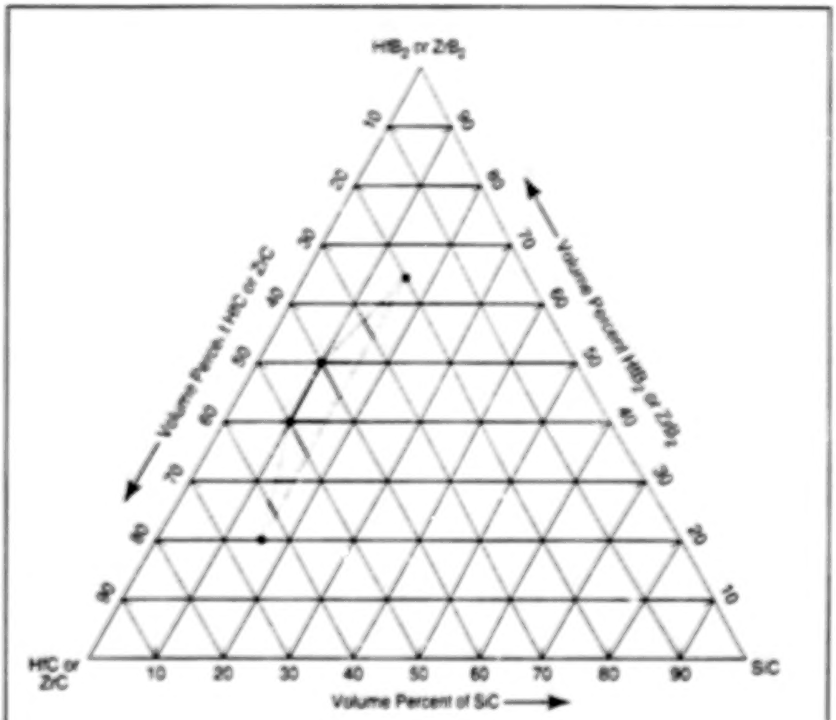

Figure 1. This **Pseudo-Ternary Phase Diagram** is for a ceramic composite of either (1) ZrB_2, ZrC, and SiC or (2) HfB_2, HfC, and SiC. The preferred composition ranges mentioned in the text are represented by the shaded trapezoidal area.

Composition in Volume Percentages		Effective Conversion Rate, µm/min.	Peak Surface Temperature, °C
64 ZrB_2 + 20 ZrC + 16 SiC	Newer Compositions	–0.98	2,020
64 ZrC + 20 ZrB_2 + 16 SiC		–6.83	2,100
80 ZrB_2 + 20 SiC	Older Compositions	–17.78	2,200
80 HfB_2 + 20 SiC		3.47	1,810

Figure 2. **Effective Conversion Rates** and peak surface temperatures are indicators of resistance to ablation. A negative effective conversion rate represents growth or effusion of oxide scale on the surface of the ceramic, while a positive effective conversion rate signifies removal and conversion of surface material.

Ames Research Center, *Michael White of White Materials Engineering, and Larry Kaufman of Cambridge Technology Center. Further information is contained in a TSP [see page 1].*

This invention has been patented by NASA (U.S. Patent No. 5,750,450). Inquiries concerning nonexclusive or exclusive license for its commercial development should be addressed to the Patent Counsel, Ames Research Center [see page 1]. Refer to ARC-12087.

Durable Advanced Flexible Reusable Surface Insulation

Blankets covered with impermeable foils are sealed loosely at their edges.

Ames Research Center, Moffett Field, California

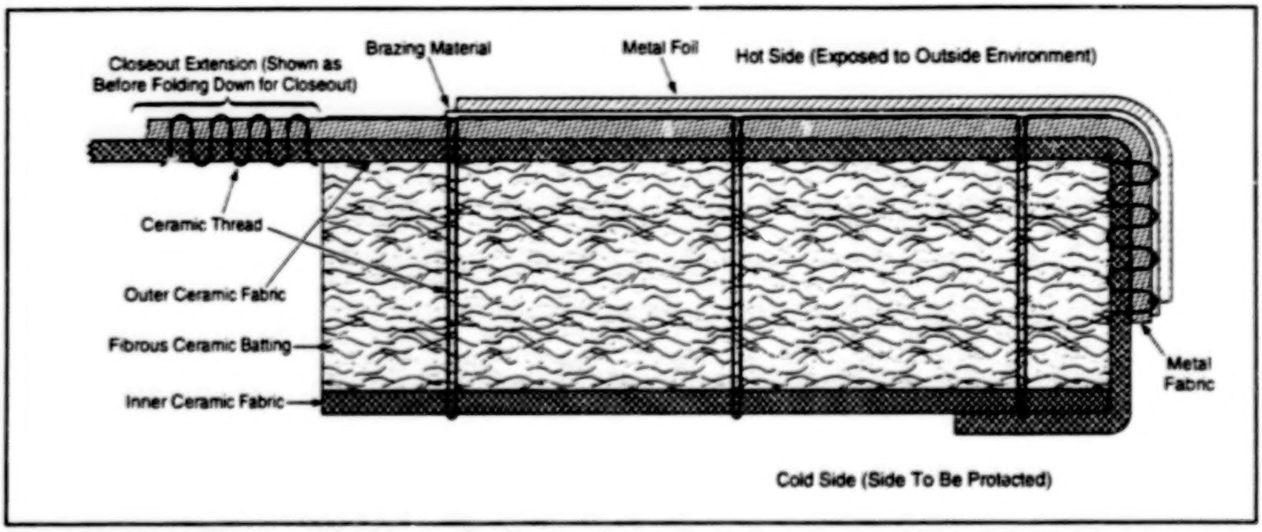

Figure 1. **This Blanket Differs From Other Insulating Blankets** in several respects, including notably the method of attachment of the outer metal foil.

Continuing efforts to develop lightweight, flexible thermal-insulation blankets that withstand high temperatures have led to design and fabrication concepts that effect the following improvements:

- Increase durability while providing adequate thermal protection to structures that would otherwise be subjected to multiple cycles of aeroconvective heating; and
- Provide for closing out the edges of insulating blankets in such a way as to minimize intrusion of water, minimize leakage of heat, provide smooth aerodynamic surfaces at joints between adjacent blankets, and accommodate thermal expansion without buckling of outer blanket surfaces.

Blankets that incorporate these improvements are denoted collectively as "durable advanced flexible reusable surface insulation," and are the latest in a series of similarly named blankets made largely of ceramic fibers.

As shown in Figure 1, a blanket of the present type includes (1) a bulk insulating layer of fibrous ceramic batting sandwiched between inner and outer ceramic fabric layers, (2) a screenlike metal fabric woven from wire, (3) an outer layer of metal foil, and (4) ceramic thread stitching. The metal fabric and foil layers are made of one or two refractory metal(s) — typically, nickel alloy(s).

In fabrication, the metal fabric, ceramic fabric, and batting layers are first stitched together as a first subassembly, using ceramic threads in a lock-stitch pattern. After stitching, the outer ceramic fabric layer is heat-cleaned. A second subassembly is then formed by attaching the metallic fabric layer to the first subassembly, and, in particular, to the ceramic fabric layer by stitching along lines that lie between the first-subassembly stitch lines. Portions of the outer ceramic and metal fabric layers protrude beyond the edges of the stitched area; these portions are stitched together with ceramic thread to form closeout extensions.

The metal-foil layer is then brazed to the metal fabric, thereby providing a relatively impermeable outer layer that helps to protect the ceramic layers against intrusion by water. Unlike in another design, there is no need to braze the metal foil to the ceramic fabric; therefore, a conventional brazing alloy can be used. (Conventional brazing alloys tend not to wet ceramic surfaces.)

After brazing, the blanket is closed out by any of three different methods, only one of which can be described in the space available for this article: A frame of fibrous refractory insulating material is placed around the periphery of the blanket. The frame can be made in sections [typically about 6 in. (≈15 cm) long] and is designed to permit flexing of the blanket on the perimeter without creating any gaps. The frame sections are attached mechanically to the surface of the structure to be protected.

Figure 2 depicts part of a frame that abuts two adjacent blanket sections. The metal-foil layer of each blanket extends onto the outer (top in the figure) surface of the frame. Pairs of rectangular opposed recesses are machined into each frame section, and rectangular openings are made in the metal-foil extensions at the locations of the recesses in the frame. A snap-fitting cover

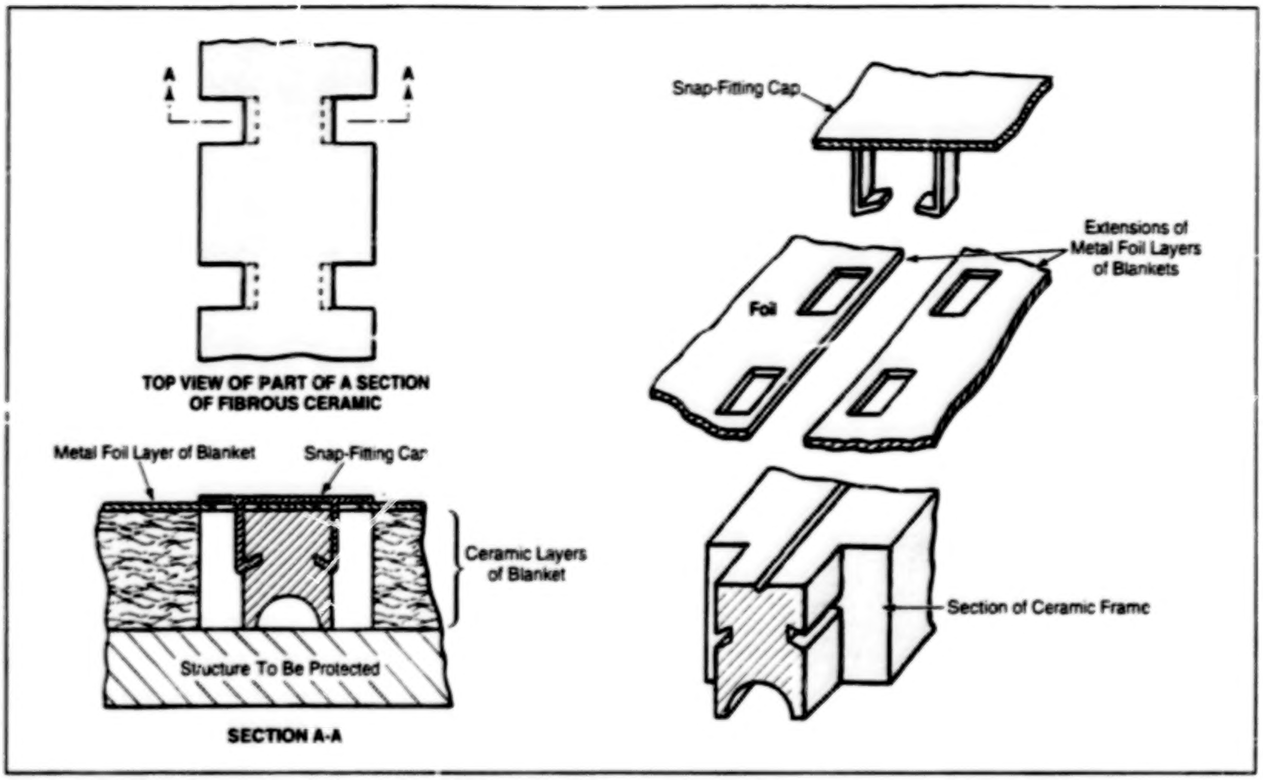

Figure 2. **Foil Extensions at the Edges of Two Adjacent Blankets** are held on the frame and sealed by the snap-fitting cap.

includes pairs of legs that extend through the openings into the recesses. The legs engage the recessed surfaces so as to secure the cover over the edge portions of the foil layers. The blankets are thus sealed on the surface by snapping in the cover.

This work was done by Daniel Rasky, Demetrius A. Kourtides, Daniel L. Dittman, Marc D. Rezin, Clement Hiel, and Wilbur C. Vallotton of **Ames Research Center**. *Further information is contained in a TSP [see page 1].*

This invention has been patented by NASA (U.S. Patent No. 5,811,168). Inquiries concerning nonexclusive or exclusive license for its commercial development should be addressed to the Patent Counsel, Ames Research Center [see page 1]. Refer to ARC-12081.

Polymeric Composite Damage Protective Overwraps for Composite Pressure Vessels

These overwraps would weigh less than conventional glass-fiber-based damage protective overwraps do.

NASA's Jet Propulsion Laboratory, Pasadena, California

Damage-tolerant polymeric composite overwraps have been proposed for lightweight pressure vessels that are made of composites of graphite fibers in polymeric matrices. Graphite-fiber/polymer composites are vulnerable to impact damage; overwraps on the pressure vessels help to protect against such damage.

In current practice, an overwrap is made of a composite of glass fibers in a polymeric matrix. The glass fibers are too weak to contribute significantly to the structural strength of the underlying pressure vessel, and the glass-fiber-based overwrap adds significantly to the weight of the vessel.

According to the proposal, the outer layers of a graphite-fiber/polymer pressure vessel would be made of polybenzoxazole (PBO) fibers in a polymeric matrix. The PBO fibers would protect the underlying graphite/polymer composite layers against impact damage, but unlike glass fibers, the PBO fibers would be almost as structurally efficient as the graphite fibers. Layers of PBO fibers could even be used as substitutes for some of the layers of graphite fibers, in which case the overwrap would contribute very little additional weight to the vessel.

This work was done by Joseph Lewis of Caltech for **NASA's Jet Propulsion Laboratory**. *No further documentation is available.*
NPO-20442

Hybrid Composite Overwraps for Low-Pressure Tanks

The weight contributed by the overwraps on the end surfaces would be reduced.

NASA's Jet Propulsion Laboratory, Pasadena, California

Hybrid versions of the high-performance overwraps used on some low-pressure tanks have been proposed. The hybrid overwraps would weigh less than do the corresponding nonhybrid overwraps, as explained below.

In current practice, the overwrap material used on all areas of a tank is a composite that contains graphite fibers. The minimum tape thickness of this overwrap material is about 0.005 to 0.007 in. (≈0.13 to 0.18 mm); consequently, the thickness of the low-angle-helical (L.A.H.) wrap on each end surface of the tank cannot be made less than about 0.010 to 0.014 in. (≈0.25 to 0.36 mm). However, thinner L.A.H.-wrap thicknesses are needed on the ends of most tanks of this type; in such cases, the excess thicknesses of carbon-fiber-based overwraps give rise to unnecessary weight penalties.

According to the proposal, the material for the L.A.H. end wraps would be a composite based on polybenzoxazole (PBO) fibers. The minimum tape thickness of the PBO-fiber-based overwrap material would be about 0.001 in. (≈0.025 mm), and the strength and elastic modulus of PBO fibers is almost equal to that of graphite fibers; as a result, no weight penalty would exist for an end wrap based on PBO fibers.

Also according to the proposal, the hoop wrap on the cylindrical portion of a tank would still be made of the conventional graphite-fiber-based composite material. This would not entail an unnecessary weight penalty because the needed hoop-wrap thickness is greater than the minimum graphite-fiber tape thickness.

This work was done by Joseph C. Lewis of Caltech for **NASA's Jet Propulsion Laboratory**. *No further documentation is available.*
NPO-20443

Repair of Composite-Overwrapped Pressure Vessels

It would no longer be necessary to replace entire expensive vessels in cases of localized damage.

NASA's Jet Propulsion Laboratory, Pasadena, California

Pressure vessels overwrapped with graphite-fiber-based composite materials that become damaged would be salvaged by a proposed repair technique. The need for the technique arises as follows: High-performance graphite-fiber-based composites are very susceptible to damage from impact or cutting. Heretofore, when a composite-overwrapped vessel has been damaged, it has been necessary to replace the vessel in its entirety. However, some vessels of this type are so large and expensive that it is uneconomical to discard them in the event of damage.

The proposed repair technique would involve adhesive bonding of a composite doubler over each damaged area. The doubler would transfer structural loads around the damaged area.

The fiber reinforcement in a doubler could be made of graphite, polybenzoxazole, or aromatic polyamid, for example. The fiber and matrix materials and the dimensions of the doubler would be chosen by design to suit the specific damaged area. The doubler would be bonded in place by use of a room-temperature-curing adhesive. Use of additional fiber overwrapping of the doubler would be determined on a case-by-case basis.

This work was done by Joseph C. Lewis of Caltech for **NASA's Jet Propulsion Laboratory**. *No further documentation is available.*
NPO-20456

Books and Reports

Properties of Cubic Boron Nitride Films

A report describes an experimental study of the surface-chemical, microstructural, and tribological properties of cubic boron nitride (c-BN) films, which are potentially useful as hard, wear-resistant coatings on bearings and on steel-cutting tools. For the experiments, BN films about 500 nm thick were synthesized by magnetically enhanced plasma ion plating onto titanium interlayers on mirror-finish silicon substrates. The films were characterized by x-ray photoelectron spectroscopy, transmission electron microscopy, electron diffraction, Fourier-transform infrared spectroscopy, atomic-force microscopy, and surface profilometry. Sliding-friction tests were performed at room temperature in vacuum, air, and underwater environments for 440C stainless-steel balls sliding on disks coated with c-BN, amorphous boron nitride (a-BN), TiN, and TiC, and for A1050 aluminum balls sliding on c-BN-coated disks. A BN film as deposited was found to comprise a c-BN layer over a hexagonal BN layer over an a-BN layer over the Ti interlayer. The c-BN surface was found to contain a slight excess of boron, combined with oxygen. In vacuum, c-BN exhibited high wear rates. In sliding against 440C steel in air and underwater, c-BN resisted wear better than the other materials did. In sliding against aluminum, c-BN exhibited high wear in air and vacuum, but little wear underwater.

This work was done by Donald R. Wheeler, Phillip B. Abel, Kenneth W. Street, and Kazuhisa Miyoshi of **Lewis Research Center** *and Shuichi Watanabe, Masao Murakawa, and Shojiro Miyake of the Nippon Institute of Technology. To obtain a copy of the report, "Surface Chemistry, Microstructure, and Tribological Properties of Cubic Boron Nitride Films," see TSP's [page 1].*

Inquiries concerning rights for the commercial use of this invention should be addressed to NASA Lewis Research Center, Commercial Technology Office, Attn: Steve Fedor, Mail Stop 4-8, 21000 Brookpark Road, Cleveland, Ohio 44135. Refer to LEW-16695.

Computer Programs

Mechanics

BLANK PAGE

Mechanics

Updated Software for Predicting Noise From Aircraft

Various measures of noise are predicted for observation points on the ground.

The FOOTPR and RADIUS computer programs implement state-of-the-art mathematical models for predicting levels of noise generated by existing or proposed aircraft. These programs can be used to calculate Federal Aviation Administration (FAA) noise-certification levels, airport-vicinity noise footprints, and levels of noise generated during climb and en route. FOOTPR and RADIUS originated in research at Lewis Research Center in the year 1981. Since that time, seven jet-noise models, four fan-noise models, a fan-noise-suppression model, and second core and turbine-noise models have been added to these codes, and a ground-reflection model already in the codes has been enhanced.

FOOTPR computes histories of noise at various observer stations (usually on the ground) for an aircraft flying at a specified set of speeds, orientations, and coordinates. These time histories are in the forms of spectra, overall sound-pressure level (OASPL), perceived noise level (PNL), and tone-weighted perceived noise level (PNLT). For each source of noise, free-field noise levels are initially computed with no correction for propagation losses other than those associated with spherical divergence. The total spectra can be corrected for the effects of atmospheric attenuation, extra ground attenuation, reflection from the ground, and shielding by the aircraft. The corresponding values of the OASPL, PNL, and PNLT are then calculated.

From the history at each point, true effective perceived noise levels (EPNLs) are calculated. Values of EPNL, maximum PNL, or maximum PNLT are thus found, as desired, for a grid of specified points on the ground.

RADIUS computes customary one-third-octave sound-pressure levels at a fixed radius at angles specified by the user. The noise-source subroutines used in RADIUS are the same as those in FOOTPR.

FOOTPR and RADIUS are batch-executed programs written in Fortran 77. No system software libraries (other than those for basic mathematical functions) are needed for execution. The current versions of these programs are executed on Unix-based computers, but they can be run on almost any computer/operating system combination that supports Fortran.

This program was written by Jeffrey Berton of **Lewis Research Center** *and Karen Kontos, Robert E. Kraft, Bangalore Janardan, and Philip Gliebe of General Electric Aircraft Engines. Further information is contained in a TSP [see page 1].*

LEW-16576

BLANK PAGE

Mechanics

Hardware, Techniques, and Processes

BLANK PAGE

36

Direct Thrust-Measurement Technique Applied to an F-15 Airplane

Preliminary results show that thrust can be measured accurately by use of strain gauges.

Dryden Flight Research Center, Edwards, California

Direct measurement of aircraft-engine thrust by use of strain gauges offers several advantages over traditional model-based methods of calculating thrust, provided that care is taken during the installation and calibration of strain gauges, and provided further that secondary load paths are understood. Advantages of the strain-gauge-based thrust-measurement method depend upon the specific engine/airframe interface, but can include the following:

- Simplification of the sensor installation, relative to the sensor suite that would be needed to support model-based calculations;
- Immunity (unlike in model-based methods) to drift and to the associated loss of accuracy as the engine deteriorates over time; and
- Excellent dynamic response.

Flight tests were performed to assess the suitability of the strain-gauge-based thrust-measurement method for application to the full flight envelope and power range of the F-15 airplane powered by F100-PW-229 engines. Other objectives of the flight tests were to determine whether unmeasurable secondary load paths affect the accuracy of this method significantly and to compare direct measurements against proven model-based thrust calculations.

Preliminary results from the flight tests showed that by properly accounting for secondary forces, and through the use of output data from a digital electronic engine-control system, excellent gross thrust-data accuracy was obtained during a subsonic-to-supersonic acceleration maneuver (see figure). Preliminary assessment of measurements throughout the remainder of the flight envelope show similar encouraging results.

At the time of reporting the information for this article, an in-depth analysis of the results from full-flight-envelope tests was planned for the near future, and the results were presented at the 1998 Joint Propulsion Conference. A description of the direct thrust sensor system, along with installation and calibration issues, were to be included in the presentation.

This work was done by Tim Conners and Robert Sims of **Dryden Flight Research Center**. *Further information is contained in a TSP [see page 1].*
DRC-98-81

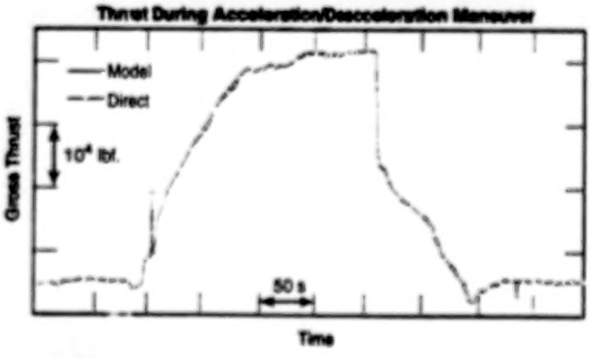

An F-15 Airplane at an altitude of 30,000 ft (9.1 km) was made to accelerate from mach 0.9 to mach 2.0, then to decelerate from mach 2.0 to mach 0.9 in a flight test of the strain-gauge-based thrust-measurement method.

Eclipse Aerotow Dynamics Experiment

Flight tests have been successful.

Dryden Flight Research Center, Edwards, California

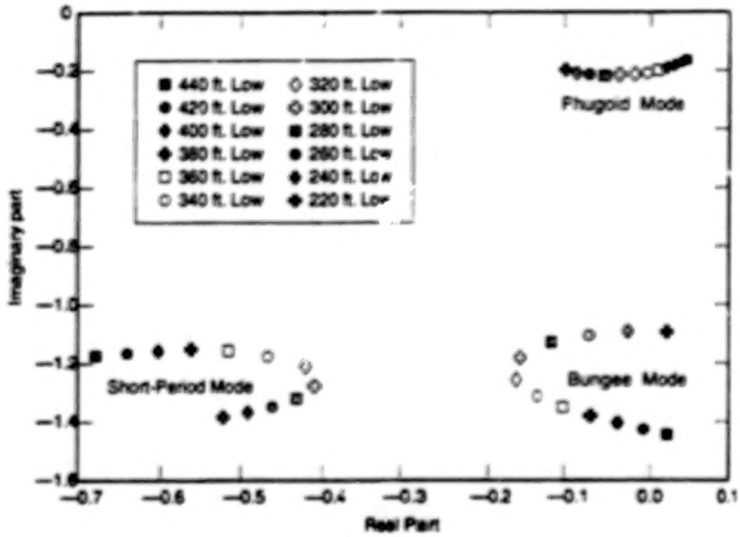

Figure 1. **Eigenvalues of Oscillations of the Tow System** in short-period, phugoid, and "bungee" (simple longitudinal) modes were identified, and a flight envelope for stable towing of the QF-106A behind the C-141A was predicted on the basis of computational simulations of the dynamics.

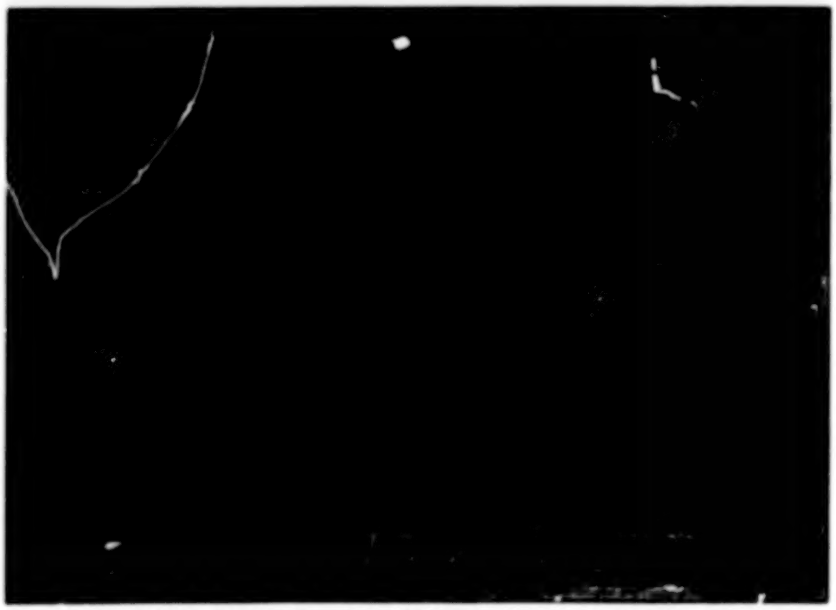

Figure 2. **The C-141A Airplane Towed the QF-106A Airplane** in flight tests. The airplanes were connected by a tow rope 1,000 ft (305 m) long.

NASA Dryden Flight Research Center is supporting a Phase II Small Business Innovation Research (SBIR) contract between the U.S. Air Force Research Labs and Kelly Space & Technology (KST). KST's innovation is to use an aerotowed reusable launch vehicle to put small satellites into low orbits around the Earth. In support of this idea, the SBIR is to demonstrate aerotow with representative aircraft; namely, a C-141A as the towing airplane and a QF-106A (a modified F-106) as the towed airplane. NASA Dryden has developed a computational simulation of the dynamics of the tow rope and towed airplane, conducted dynamic-stability studies, developed test plans, and completed successful ground, taxi, and flight tests.

Towing a launch vehicle to altitude should make it possible increase the payload and decrease the cost of the launch. No previous aerotow experiments produced tow-dynamics data of any consequence. Dryden's expertise in conducting unusual flight tests was needed to perform simulations of the dynamics (see Figure 1), determine a safe flight-test approach, and conduct the aerotow flight tests.

Dryden provided support for the modifications that were made in converting the F-106 into the towed experimental airplane, and for its operation and maintenance. Dryden also provided research instrumentation, the test range, flight-safety, operations, research pilots, and research engineering analysis of the aerotow system. The Air Force Flight Test Center also supported this project by providing the C-141A airplane and flight crew.

Tests of the entire tow system (see Figure 2) have been completed. These included high-speed taxi (through rotation of the QF-106A airplane) and successful flight tests.

The results of the tests showed that, among things, the tow rope is not a straight line as previously assumed. The rope exhibits considerable sail from the airflow. Observed stability boundaries do not match those predicted from the simulations; with a differential altitude of approximately 200 ft (60 m) between the aircraft, the tow-rope tensions were stable. The rope sail also alters the trim of the aircraft relative to the predictions from the simulations; the angle at the point where the rope meets the QF-106A was found to be more acute than it was predicted to be, making it necessary to use more elevon deflection. Analysis was continuing at the time of reporting the information for this article.

This work was done by Al Bowers and Jim Murray of **Dryden Flight Research Center.** *Further information is contained in a TSP (see page 1).*

DRC-98-79

Machinery

Hardware, Techniques, and Processes

Books and Reports

BLANK PAGE

Experiment on Quasi-Tailless Flight of an X-31A Airplane

Lessons learned will be applied in future development of thrust vectoring.

Dryden Flight Research Center, Edwards, California

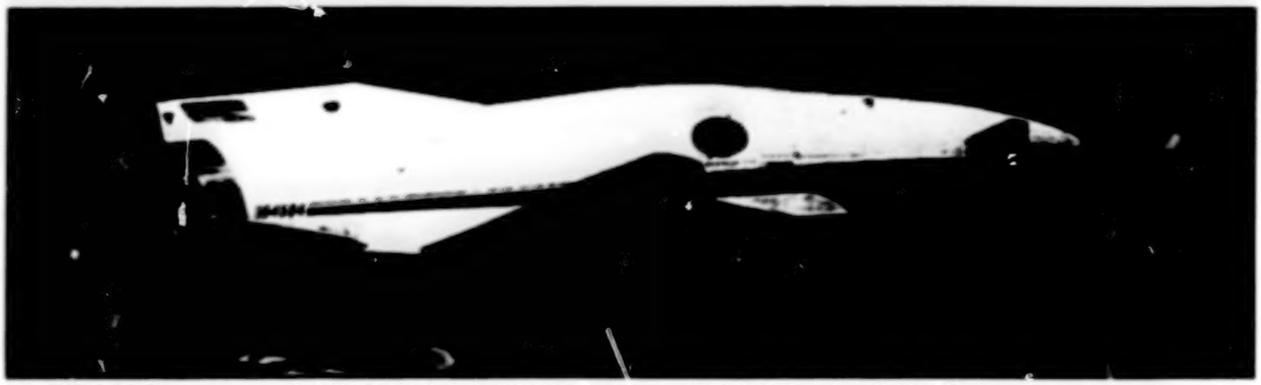

The X-31A Airplane was operated with thrust vectoring in a quasi-tailless mode to test and demonstrate advanced control concepts.

An experiment consisting of flight tests on the X-31A airplane (see figure) has demonstrated the ability to use thrust vectoring to replace the functions of stabilization and turn coordination usually required of a rudder and vertical tail. Comments by the pilot indicated no differences in handling qualities for the majority of the tests flown. The experiment showed that the greatest demand was placed on the thrust-vectoring system at low thrust settings and high roll accelerations. It was demonstrated that a higher level of interaction between the engine and flight-control system will be needed for future reduced-tail or tailless aircraft with thrust-vector control. This experiment helped to introduce thrust vectoring as a new design dimension for future aircraft.

The quasi-tailless concept involves the use of in-flight simulation to assess the effect of partial to total removal of the vertical tail; in implementing this concept in the experiment, the rudder control surface was used to cancel the stabilizing effects of the vertical tail. Yaw-thrust-vector deflections were used to restabilize and control the aircraft. The quasi-tailless mode was flown supersonically with gentle maneuvering. Precise approaches and ground attack profiles were flown subsonically with more aggressive maneuvering.

The supersonic quasi-tailless test showed that maneuvers typically required of transport aircraft could be controlled by thrust vectoring for fairly high levels of instability. A tail-reduction setting of 70 percent was used during part of the experiment and was found to be equivalent to an instability-amplitude-doubling time of approximately 170 ms. The fidelity of the sideslip feedback measurement was found to be a critical factor in determining the amount of destabilization achieved by the quasi-tailless system. The sideslip feedback path included an equivalent delay of approximately 67 ms from complimentary filtering of flight-test-boom and inertial parameters, and a deadband caused by misaligned dual redundant sideslip vanes. These factors both influenced the level of destabilization achieved in flight.

To accomplish the objectives of the subsonic tests, it was necessary to maneuver the airplane more aggressively. The precise-approach tests provided a first look at the use of thrust vectoring as a primary means of control at low power settings. The flying qualities were found to be independent of tail-reduction setting up to a setting of 50 percent (an instability-amplitude-doubling time of about 0.92 s). High throttle activity coupled with a lag on the thrust-estimation algorithm resulted in errors in the thrust-control loop gain as high as 4 dB. Because of the high loop-gain margin of the X-31A, these errors did not produce any noticeable stability problems. The tests showed that an accurate and redundant on-board thrust-estimation algorithm is necessary in an integrated propulsion/flight-control system. Either the design of such a system should provide for better estimation of thrust changes resulting from rapid throttle movements, or else a high stability margin for the thrust-vector control loop should be required.

All precise approaches were flown in clear air. A limited nonlinear simulation study showed that even with the deadband and lag in the sideslip feedback path, no significant handling-qualities problems were introduced with simulated turbulence. The issues of ride qualities and rejection of disturbances in the presence of atmospheric turbulence would be better addressed with a real tailless or reduced-tail vehicle. Because of limitations on frequency response and fidelity, the in-flight quasi-tailless system is not accurate enough to reproduce the true directionally unstable behavior characteristic of the response of an aircraft to turbulence.

A reasonable approach to the engine-out failure condition must be developed. If this approach is to include emergency devices that would be deployed to regain directional stability, then the cost, weight, and complexity of such devices must be considered. The cost and weight of adding a thrust-vector system is being reduced by production of axisymmetric thrust-vectoring engines. The X-31A quasi-tailless flight test experiment showed that tailless and reduced-tail fighter-type airplanes are feasible. When the thrust-vectoring capability and reduced-tail configuration are incorporated into the design from the beginning, the benefits of lower drag, reduced structural complexity, and reduced radar cross section could, potentially, outweigh the concomitant added complexity.

This work was done by John Bosworth and Patrick Stoliker of **Dryden Flight Research Center**. *Further information is contained in a TSP [see page 1].*
DRC-96-12

NASA Developing Crew-Return Vehicle

The spacecraft equivalent of a lifeboat will be available to astronauts.

Dryden Flight Research Center, Edwards, California

NASA photo by Jeff Doughty

The X-38 CRV is shown here under the wing of a B-52 airplane.

Up a creek without a paddle? Not if you're an International Space Station astronaut with a CRV. That's short for Crew Return Vehicle, and it's being developed following an innovative approach in the X-38 program. The CRV will perform three specific roles:

- A lifeboat if the space station becomes uninhabitable;
- An ambulance if a crewmember becomes sick or injured; and
- A way home if the space shuttle is unavailable.

The CRV is a 30-ft (9.1-m) long spacecraft that will be moored on the station and will carry up to seven crewmembers safely back to Earth. Designed to replace the three-person Soyuz vehicle used in early space-station operations, it is completely autonomous, can carry the entire station crew, has significant cross-range capability, and can make ground-based, low-speed, soft landings at predefined sites around the world by use of a large parafoil.

In response to Administrator Dan Goldin's challenge to build a new spacecraft to transport humans in a better, faster, cheaper way, engineers at NASA's Johnson Space Center conceived the X-38 program to solve the technical issues associated with the development of the CRV. The X-38 program relies on a series of low-cost, unpiloted development vehicles to perform flight demonstrations of innovations to be incorporated into the CRV. Paramount among the innovations is the parafoil and its control mechanisms. The proper selection of innovations makes it possible to build and test the prototype CRV quickly; as a result, the experience needed for designing and building the CRV can be gained early in the development cycle. A total of five vehicles will be used to test various parts of the eventual CRV mission.

The first of the X-38 vehicles successfully made its maiden flight in March 1998 at Dryden Flight Research Center. Launched from Dryden's venerable B-52 mother ship at an altitude of 23,000 ft (7 km), the vehicle known as V131 deployed a drogue parachute and parafoil on cue and glided to a soft landing on the Precision Impact Range Area at Edwards Air Force Base. The flight marked the first time a parafoil of this size (larger than the B-52 wing area) had been deployed from an aerodynamic-lifting-body aircraft. Although some minor problems were encountered, the test demonstrated the feasibility of the parafoil concept.

Like the familiar wedding couplet — "Something old, something new" — the X-38 blends proven technology with state-of-the-art technology. The basic lifting body shape is derived from the X-24A program tested at Dryden in the 1960s and 1970s. Data on re-entry aerodynamics and heating were recovered from flights in the X-23 pro-

gram undertaken by the Air Force in the mid-1960s. Flight-proven components from the space shuttle have been used to reduce risk wherever possible. Conversely, the parafoil, electromechanical flight surface actuators, and fiber-optic systems are all examples of emerging technology being used to augment CRV capabilities. The use of the parafoil provides a low-speed, soft-landing capability without the need for a pilot or a prepared runway. Unlike traditional hydraulic actuators, the electromechanical actuators afford a leak-free, non-freezing capability for the intended three-year stay of the CRV at the station.

To increase the likelihood of a successful X-38 program, the Johnson Space Center X-38 team has enlisted several partners. In addition to providing the B-52 launch capability, Dryden has assisted with flight controls and flush air-data systems advice, and general flight-test and range-safety expertise. Pioneer Aerospace Corporation has led the development of the parafoil, and the Army has provided test facilities at Yuma Proving Ground. In an example of an international cooperative effort, the European Space Agency and the German National Space Agency will provide several components for the first space flight of the X-38, to be launched from the Space Shuttle in November 2000.

Ideally, the CRV will never be used for a real emergency. However, the recent problems with the Mir space station illustrate the need for a way home, just in case. The CRV will be there for astronauts in case they need it.

This work was done by John F. Muratore of Johnson Space Center and Christopher J. Nagy of **Dryden Flight Research Center.**
DRC-98-90

Books and Reports

Active Homopolar Magnetic Bearing

A report presents information on an earlier work on active magnetic bearings with high-critical-temperature superconducting coils. To recapitulate, the device is a homopolar radial-type active magnetic bearing with a bias coil and control coils made of a high-critical-temperature superconductor. The report discusses major features of the design and operation of the bias and control coils, measurements of ac power losses in the control coils, and results of experiments in which the device was operated at the temperature of liquid nitrogen. The experimental findings and conclusions stated in the report are nearly identical to those noted earlier. One particularly notable conclusion is that ac losses appeared to be related to coil inductances and that it may therefore be possible to reduce these losses by winding the control coils from twisted, multifilamentary forms of the superconductor.

This work was done by G. V. Brown, E. DiRusso, and A. J. Provenza of **Lewis Research Center**. *To obtain a copy of the report, "An Active Homopolar Magnetic Bearing With High Temperature Superconductor Coils and Ferromagnetic Cores," see TSP's [page 1].*

Inquiries concerning rights for the commercial use of this invention should be addressed to NASA Lewis Research Center, Commercial Technology Office, Attn: Tech Brief Patent Status, Mail Stop 7-3, 21000 Brookpark Road, Cleveland, Ohio 44135. Refer to LEW-16419.

BLANK PAGE

Fabrication Technology

Hardware, Techniques, and Processes

BLANK PAGE

Crimping Thin PTFE Tubes Onto Thin Stainless-Steel Tubes

Crimps prove superior to wrapped wires, flared tubes, ringed hose barbs, and the like.

Lewis Research Center, Cleveland, Ohio

Figure 1. The **Crimping Tool** is a modified pair of crimping pliers containing a hexagonal crimping die. The hexagon was chosen over other shapes because it minimizes the amount of copper extruded from the sleeve during the crimping process.

Figure 2. A **Crimped Connection** made by the present technique grips more strongly than does a connection made by the traditional twisted-wire technique. One reason for the superiority of the present technique is that the grip is spread over a larger area.

A crimping technique has been developed for fastening polytetrafluoroethylene (PTFE) tubes of 0.032-in. (0.81-mm) outside diameter and 0.0105-in. (0.267-mm) inside diameter onto stainless-steel hypodermic tubes of 0.0105-in. (0.267-mm) outside diameter. The technique was developed to provide lightweight connections that would not slip or leak when subjected to rapid, repeated movements. The technique is needed because connections made with such conventional means as wrapped and/or twisted wires, flared tubes, ringed hose barbs, and combinations of these eventually slip and/or leak when handled or moved repeatedly.

The development of the technique included tests that revealed that the best crimp reduction for PTFE is about 18 percent. The dimensions of the crimping sleeves and the crimping tool were chosen accordingly. The crimping sleeves were made from copper rods of 0.047-in. (1.2-mm) diameter, cut to 1/8-in. (3-mm) length, and drilled to an inside diameter of 0.033 in. (0.84 mm). The crimping tool was made by machining a pair of crimping pliers down to a thickness of about 0.100 in. (2.54 mm) and cutting a 0.038-mm (0.97-mm) hexagonal crimping die into its tip (see Figure 1).

Optionally, one can prepare the crimp area on the stainless-steel tube with a light grit blast prior to joining to improve the subsequent grip on the tube. To make a connection, one first slips the copper crimping sleeve over the PTFE tube, then inserts the stainless-steel tube into the PTFE tube a sufficient distance to enable proper positioning of the crimping sleeve as described next. The crimping sleeve is positioned so that PTFE and stainless-steel tube segments 0.05 to 0.06 in. (1.3 to 1.5 mm) long protrude from opposite ends of the crimping sleeve. The tool is then applied to effect the crimp. Figure 2 shows a completed connection.

Limited experience thus far seems to indicate that a connection made by this technique does not leak measurably when exposed to vacuum or to pressure up to 115 psi (0.79 MPa). The technique can readily be modified, by appropriate changes in dimensions of the sleeves and tool, for PTFE and stainless-steel tubes of different diameters. Potential uses for this technique could include joining fuel lines for gas-powered models, joining pneumatic and gas lines in general, and perhaps joining tubes in medical equipment.

This work was done by Myron M. Joseph (retired) and George J. Saad of **Lewis Research Center**. *Further information is contained in a TSP [see page 1].*

Inquiries concerning rights for the commercial use of this invention should be addressed to NASA Lewis Research Center, Commercial Technology Office, Attn: Tech Brief Patent Status, Mail Stop 7-3, 21000 Brookpark Road, Cleveland, Ohio 44135. Refer to LEW-16689.

Making Curved Diffractive Optics by E-Beam Lithography

Substrates need not be flat, and grating lines need not be straight.

NASA's Jet Propulsion Laboratory, Pasadena, California

Electron-beam (e-beam) lithography has shown promise as a technique for fabricating diffractive optical elements on nonflat substrates. Such optical elements could include convex or concave diffraction gratings with curved grating lines, for use in imaging spectrometers or other scientific instruments operating at wavelengths from ultraviolet through midinfrared.

Heretofore, diffractive optical elements made, variously, by diamond ruling and optical holography, have been available commercially on flat substrates only. The lines in these gratings have been straight or else have had modest, regular curvatures

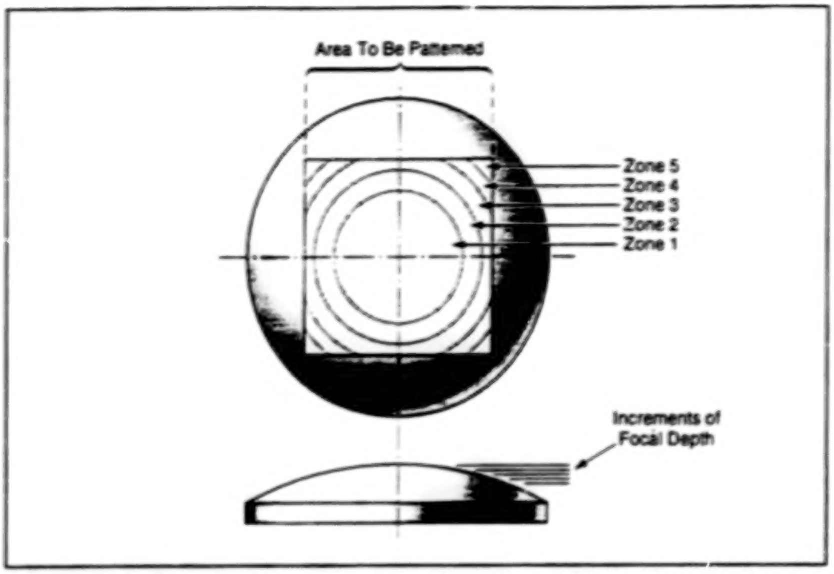

A Substrate To Be Patterned by electron-beam lithography is partitioned into zones of different focal depth, in essentially the same manner in which elevation contours are formed on a topographical map. An electron-beam subpattern exposure is then performed in each zone.

at most. In contrast, diffractive optical elements made by electron-beam lithography can have arbitrary line shapes and/or arbitrary phase functions.

The present electron-beam-lithographic technique is an extension of another, recently developed electron-beam-lithographic technique for writing phase holograms into thin films of poly(methyl methacrylate) on flat substrates. By patterning and otherwise controlling the electron-beam exposure and monitoring the development/etching process until precise depths are achieved, one can adjust optical phase delays to a precision of less than 1/50th of a wavelength, within 0.5-μm square regions. Devices produced by use of this technique on flat substrates include Fresnel lenses, arrays of Fresnel lenslets, gratings with both straight and curved grooves, holograms that yield gray-scale images, and patterns for free-space optical interconnections.

Application of the technique to a concave or convex substrate (see figure) involves the following sequence of steps:

1. Establish a grid of points on the substrate.
2. For each grid point, determine the electron-beam-apparatus focus, rotation, and deflection calibration values.
3. From the values obtained in step 2, determine the depth of focus over which patterning errors can be considered negligible, and use the depth-of-focus information to define depth zones.
4. Partition the exposure pattern into subpatterns — one subpattern for each depth zone.
5. Using the electron-beam apparatus, expose each depth zone according to its subpattern. Readjust the apparatus, as needed, when proceeding to the next subpattern.

The technique has been demonstrated by using it to form a small prototype diffraction grating on a convex spherical substrate. In a test, the grating exhibited a first-order-diffraction efficiency of 88 percent. There was no evidence of degradation of the grating by curvature of the substrate. The prototype grating was small. Continuing development efforts are directed toward increasing the patterned area and decreasing the amount of light scattered (as distinguished from diffracted) by gratings of this type.

This work was done by Paul Maker, Richard Muller, and Daniel Wilson of Caltech for **NASA's Jet Propulsion Laboratory**. *Further information is contained in a TSP [see page 1].*

In accordance with Public Law 96-517, the contractor has elected to retain title to this invention. Inquiries concerning rights for its commercial use should be addressed to

Technology Reporting Office
JPL
Mail Stop 122-116
4800 Oak Grove Drive
Pasadena, CA 91109
(818) 354-2240

Refer to NPO-20296, volume and number of this NASA Tech Briefs *issue, and the page number.*

Integrally Wound Skirt for Composite-Overwrapped Tank

Strength would be increased and weight reduced.

NASA's Jet Propulsion Laboratory, Pasadena, California

The skirt that supports a composite-overwrapped tank would be made an integral part of the composite overwrap, according to a proposal. In current practice, the structure that supports a composite-overwrap tank usually includes a layer of rubber between the tank and its skirt. The rubber layer is heavy and constitutes a relatively weak link in the tank-supporting structure.

The proposal arose from an investigation of how to reduce the weight of the tank and its supporting structure, considering the tank as part of an overall tank/structure system. The investigation revealed that elimination of the rubber layer could reduce the weight of the system considerably.

The fiber reinforcement in the skirt would be filament wound directly onto the tank, without an intervening layer of rubber. The weight of the tank/structure system would be reduced and the strength of the skirt/tank bond increased accordingly, and the skirt would bear part of the hoop stress of the tank.

This work was done by Joseph C. Lewis of Caltech for **NASA's Jet Propulsion Laboratory**. *No further documentation is available.*
NPO-20455

Life Sciences

Hardware, Techniques, and Processes

BLANK PAGE

Improved Suit for Protection During Abrasive Blasting

Less time is spent in preparation and cleanup.

John F. Kennedy Space Center, Florida

An improved suit to be worn by a worker during abrasive blasting has been developed. Denoted an environmentally controlled abrasive-blasting suit (ECAB), it provides comprehensive protection that, heretofore, has been afforded by a set of special under- and over-garments (including a helmet) and a respirator. These garments and the respirator must be donned in a time-consuming "suit-up" procedure before abrasive blasting. After blasting, the worker must not only doff the garments and respirator but must also shower and the garments must be laundered before they are used again. In contrast, donning the ECAB takes less "suit-up" time, there in no need to wear special undergarments inside the ECAB, there is no need for a respirator, it is not necessary to shower after doffing the ECAB, and the suit does not require laundering prior to reuse.

The ECAB (see figure) is an ensemble that forms a closed envelope to isolate the worker from the hazards of the abrasive-blasting environment. The design of the ECAB also reflects a concern for mobility and comfort to increase the worker's endurance. The ensemble includes a helmet, a coverall, detachable gloves, detachable boots, plus detachable hoses and a manifold for supplying and distributing air for both breathing and cooling. The helmet features a transparent visor and disposable blast shields.

The ECAB Protects the Worker from the hazards of abrasive blasting, and offers advantages over older, multiple-garment protective ensembles.

The arms and legs of the coverall terminate in special cuffs designed for attachment and detachment of the gloves and boots. A similar provision is made for attachment and detachment of the helmet. The coverall materials are capable of withstanding impacts by abrasive particles that bounce back from the workpiece. The gloves are flexible enough to enable the worker to operate the abrasive-blasting equipment with ease. The boots are soled and sized to accept safety shoes or boots.

All attachment/detachment cuffs include seals to prevent the entry of abrasive particles into the suit. Relief valves allow air to flow out of the suit but resist the inflow of atmospheric air, thereby helping to maintain a slight positive pressure of supplied air within the suit.

The ECAB is designed and built to provide long-term multiple use.

This work was done by Raymond A. Anderson and Robert E. Persson formerly of EG&G Florida, Inc., for **Kennedy Space Center**. *Further information is contained in a TSP [see page 1].*

Inquiries concerning rights for the commercial use of this invention should be addressed to the Technology Programs and Commercialization Office, Kennedy Space Center, (407) 867-6373. Refer to KSC-11868.

Exoskeletal System for Neuromuscular Rehabilitation

This system could help a neurally impaired patient regain the ability to walk.

NASA's Jet Propulsion Laboratory, Pasadena, California

A system of sensors and actuators designed to fit on the lower extremities of human patients and astronauts like an exoskeleton is under development to serve diverse purposes in neuromuscular research and rehabilitation. This system will be operated under both Earth and microgravity conditions. A product of integrated research efforts in several fields of science and engineering, the design of the system incorporates advances in microsensors, robotics, and mathematical modeling of the dynamics of walking. The design of the system has been guided by research findings that show that the spinal cord (even when cut off from the brain by injury) is capable of relearning the ability to walk.

The system could be used by an astronaut exercising in space under the conditions of microgravity to help maintain normal locomotion skills, muscle mass, and bone calcium levels. On Earth, the same system could be used for the rehabilitation of stroke or spinal-cord-injured patients in an effort to restore part or all of their ability to walk.

At present, one way to perform such rehabilitation is to suspend the patient in a harness over a treadmill so that their legs bear only part of their entire weight while therapists manipulate the patient's legs to assist in stepping on the running treadmill. As the patient gains more ability to step, the amount of assistance needed is decreased. The disadvantages of this approach are several: a limited number of therapists can assist only a small number of patients, the assisted movements are only approximations of normal stepping motions, and there is no way to quantify changes in the amount of assistance needed. Thus, there is a need for something that can accurately measure limb motions, apply and measure controlled forces and torques, and be used to manipulate an entire leg in normal kinematic patterns and speeds. Such a device could be used to study more subjects with greater thoroughness and precision, and could make it possible to rehabilitate more patients with higher levels of success than

can now be attained with human assistance alone. Such a robotic device could also be used to preserve normal locomotion skills for astronauts during long-term microgravity conditions.

The present exoskeletal system is a prototype of such a robotic device. Encouraging results have been obtained in preliminary tests performed on humans in the Neurological Rehabilitation and Research Unit of the University of California at Los Angeles. When the system is fully developed, continuous analysis and control of the force and torque actuators needed for normal walking motions will be generated from a combination of dynamical motion modeling and sensory feedback from the exoskeleton.

Thus, the development of the exoskeletal system involves the parallel development of sensors capable of measuring six degrees of freedom and computational resources capable of instantaneous analysis and control. This approach uses the exoskeleton to control and monitor the movements of each segment of the lower limb during locomotion and a mathematical model that accounts for such details as the masses and kinetics of limbs and the moment arms of individual muscles of the knee, hip, and ankle. Variables that can be investigated by use of the model include the percent of body weight loading, the frequency of stepping, the speed of walking, and changes in muscle output that would occur in hypertrophy or atrophy.

This work was done by James Weiss, Antal Bejczy, Bruno Jau, and Gerald Lilienthal of Caltech for **NASA's Jet Propulsion Laboratory**. *Further information is contained in a TSP [see page 1].* *NPO-20370*

END

DATE FILMED

07-02-99